An Operational, Diagnostic Surface Energy Budget Model

TODD M. CRAWFORD AND HOWARD B. BLUESTEIN

School of Meteorology, University of Oklahoma, Norman, Oklahoma

(Manuscript received 22 February 1999, in final form 15 August 1999)

ABSTRACT

In recent years, there has been a growing appreciation of the importance of land–atmosphere interactions in determining the state of the boundary layer. To examine this phenomenon in more detail, a new technique has been developed to evaluate the surface energy budget during the daytime from standard meteorological observations. Using only Oklahoma Mesonetwork (Mesonet) data at 5- and 30-min intervals as input, the technique calculates net radiation (R_n), ground heat flux (G), and latent heat flux (LE). The sensible heat flux (H) is calculated as a residual. The R_n term is calculated using observed values of downwelling shortwave radiation, an improved method of estimating downwelling longwave radiation, and simple parameterizations of upwelling shortwave and longwave radiation. The modeled values of R_n are unbiased and are consistently within 25 W m^{-2} of observed values. Ground heat flux, which is the combination of a 5-cm soil flux term and a storage term, was difficult to verify without prior knowledge of vegetation height. Latent heat flux is calculated from the Penman–Monteith equation, in which surface resistance is estimated. Using data from the Atmospheric Radiation Measurement Program, simple parameterizations were developed (one each for eastern and western Oklahoma) for this term, based on observations of temperature, relative humidity, solar radiation, soil moisture, and estimates of leaf age.

Net radiation and G are calculated, and then their sum is partitioned into H and LE. Because there were no observations of LE at the Mesonet sites, the preexisting reliable estimates of H were used to verify the new estimates of both H and LE. Because there were problems with the soil moisture data from some of the sites, data from only two Mesonet sites were available for verification. The estimates of H were unbiased and within 60 W m^{-2} (rmse) at the sites in both eastern and western Oklahoma. Because of the limited verification data currently available, the model results are preliminary and in need of further testing.

1. Introduction

Over the past few decades, there have been great strides made in the ability to predict synoptic-scale motions in the atmosphere as a result of improvements in numerical models. In recent years, mesoscale and storm-scale models have shown great promise in resolving and predicting atmospheric phenomena such as sea breezes (Hjelmfelt 1990; Sousounis and Fritsch 1994), drylines (Ziegler et al. 1995; Crawford and Bluestein 1997), and lake-effect snows (Anthes 1978; Arritt 1989). The current state of computing power and speed, however, still is insufficient for modeling some of the fundamental processes in the atmosphere. In particular, one important problem that mesoscale and storm-scale models must address is how to simulate the combination of atmospheric processes that accounts for the development of cumulus convection in some locations but not in others. Horizontal variations in surface energy fluxes may play a vital role in determining where convection occurs.

Numerous land surface schemes have been developed to model the biosphere–atmosphere interaction more accurately. The Project for Intercomparison of Land Surface Parameterization Schemes (PILPS; Henderson-Sellers et al. 1995) compared 23 of these schemes using a 1-yr dataset (both forcing and validation) from Cabauw, Netherlands (Chen et al. 1997). All schemes used the same forcing data, but the variation in the resulting flux predictions was significant. The range of annual mean values among the schemes for predicted net radiation, sensible, and latent heat fluxes was 10, 30, and 25 W m^{-2}, respectively. Many of the schemes tested are designed for coupling to atmospheric models with scales ranging from mesoscale to global. More recently, Xu et al. (1999) and Zhou and Xu (1999) used a variational method to calculate surface fluxes using data from the Atmospheric Radiation Measurement Program (ARM; Stokes and Schwartz 1994) and the Oklahoma Mesonetwork (Mesonet; Brock et al. 1995), respectively. Most of these schemes incorporate complex, nonlinear treatments of soil and plant processes, are computationally intensive.

Corresponding author address: Todd M. Crawford, Cooperative Institute for Mesoscale Meteorological Studies, National Severe Storms Laboratory, 1313 Halley Circle, Norman, OK 73069.
E-mail: tcrawford@ou.edu

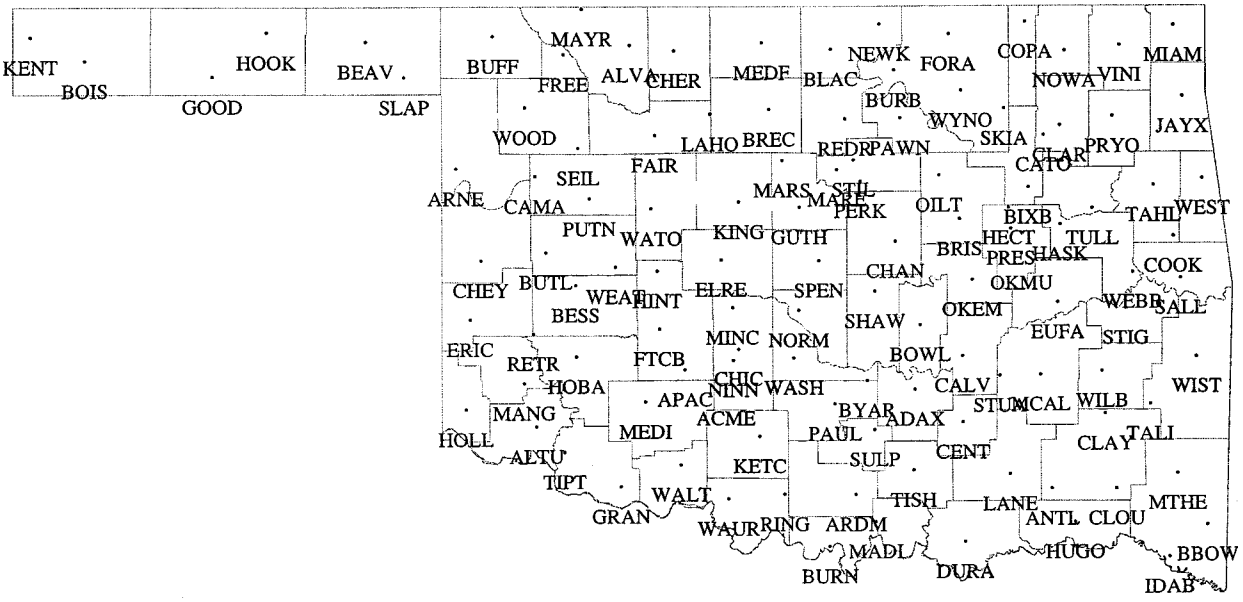

FIG. 1. The 116 stations of the Oklahoma Mesonetwork that record solar radiation, air temperature, relative humidity, wind speed and direction, and rainfall at 5-min intervals.

Recent advances in observational capability provide an opportunity to calculate surface energy fluxes in real time. The Mesonet consists of 116 automated surface observing stations distributed across the state. These stations record incoming solar radiation, air temperature, relative humidity, wind speed and direction, soil temperature, barometric pressure, and rainfall at 5-min intervals (Fig. 1). The average station separation of ~30 km provides a unique real-time opportunity to detect surface features in Oklahoma at much smaller spatial and temporal scales than was previously possible. Unfortunately, the operational, high-resolution surface data set provided by the Mesonet is not duplicated aloft, where rawinsondes are launched only twice daily at a greatly reduced horizontal resolution. Thus, the use of this surface dataset is of crucial importance in determining the characteristics of the planetary boundary layer. McGinley (1986) noted that ''the ability to acquire information has outstripped the ability to assimilate it at the local level.'' The goal of this paper therefore is to describe a relatively simple diagnostic model that will calculate surface energy fluxes in real-time using Mesonet data as input. It is hoped that this model eventually will be used to improve the limited understanding of convective initiation.

2. Background

The First Law of Thermodynamics states that energy can be neither created nor destroyed but only converted among different forms. At the interface between the earth and its atmosphere, an exchange of energy occurs from radiative, convective, and conductive processes. Radiative energy is transferred by photons moving through the atmosphere at the speed of light. Convective energy is transferred from the surface to the lower atmosphere by the turbulent vertical motion of the air. Conductive energy is transferred by molecular collisions in the soil. The latter mode of transfer is much more effective in solids than in either liquids or gases (Oke 1987), although conduction does also occur in the atmosphere just above the surface.

The total energy input to the surface from the atmosphere must be either stored in the soil or returned to the atmosphere. The net radiative energy flux at the surface (R_n), that is, the difference between the sum of the downwelling shortwave (SW_d) and longwave radiation (LW_d) and the sum of the upwelling shortwave (SW_u) and longwave (LW_u) radiation, is converted into three dominant forms of ''output'' energy. Two forms are characterized by convective exchange of heat (sensible heat flux, H) and of moisture (latent heat flux, LE), and the third is characterized by conductive exchange (ground heat flux, G). Thus, the surface energy balance (Fig. 2) is

$$R_n = H + \mathrm{LE} + G. \tag{1}$$

For this study, the effective ''surface'' is located at the aerodynamic roughness length (z_{0m} for momentum, z_{0h} for heat and moisture), which will be detailed later in this section. For this study, positive values of the fluxes refer to energy transfer in the direction of the arrows in Fig. 2, which is consistent with the convention of denoting radiative (nonradiative) fluxes as positive when directed toward (away from) the surface (Garratt 1992).

Many different methods have been employed to estimate the turbulent fluxes (H and LE). Remote sensing

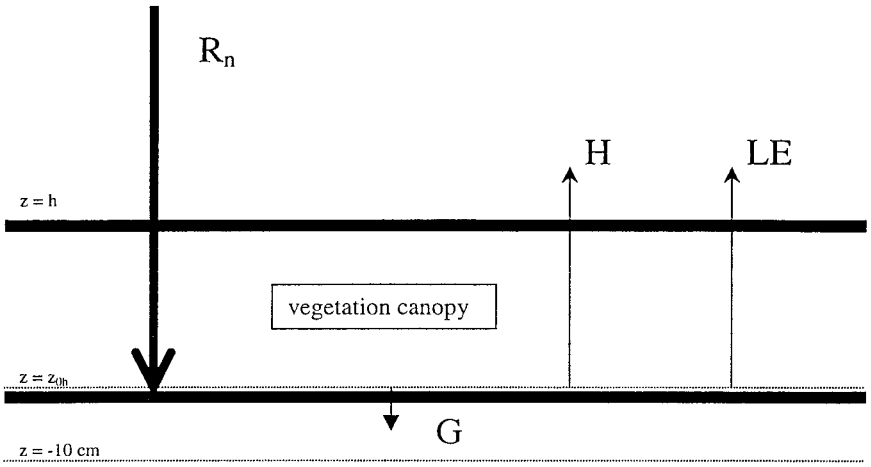

FIG. 2. Illustration of surface energy balance on a typical afternoon. The vegetation canopy is located between the thicker solid lines. The aerodynamic roughness length of heat and moisture is represented by z_{0h}. Positive values of the fluxes refer to energy transfer in the direction of the arrows.

is the most versatile and rigorous method, because satellites can detect radiance with a very high spatial resolution relative to current surface observing networks. This method, however, has three major problems. First, the measured satellite radiance must be corrected for atmospheric and geometric effects before the surface fluxes can be extracted. Atmospheric effects generally refer to the transmissivity of the atmosphere at a normal range of terrestrial temperatures, which is inversely proportional to the amount of water vapor in an atmospheric column (Schmugge and Becker 1991). Second, this method will only produce accurate readings during periods of clear skies, which greatly limits the utility of the flux calculations. Third, satellite grid points are averaged and are not necessarily representative of any particular Mesonet site. Because of this fact, it was decided that H and LE must be estimated based on near-surface observations alone.

There are three general approaches used in estimating sensible and latent heat fluxes at the land surface: the eddy fluctuation method, the profile method, and the resistance method (Oke 1987). The eddy fluctuation method (Businger et al. 1990) requires specialized, fast-response instruments that can detect transient perturbations in vertical velocity, temperature, and vapor pressure. Use of this method requires data postprocessing and this fact, along with the considerable expense of the instrumentation, renders this method inapplicable in an operational environment.

The profile method is based on the assumption that the surface layer is a constant-flux layer. Based on this assumption, calculation of surface sensible and latent heat fluxes requires measurement of air temperature, humidity, and wind at two or more levels within the surface layer. About half of the Mesonet sites are equipped with temperature sensors at two levels. However, the temperature sensors at the two levels are dissimilar. Even if the observational error associated with each sensor were negligible, a small bias in one of the sensors (e.g., from different calibration standards) would render the flux calculations grossly inaccurate.

The third method, referred to as the resistance or Penman–Monteith (PM) method (Penman 1948; Monteith 1965), is also called the Combination Model (Oke 1987), because it combines a parameterization for R_n and G in the surface energy balance with the PM approach of partitioning the available energy ($R_n - G$) into sensible and latent heat fluxes. This method requires only one level of data so that all 116 Mesonet sites can be utilized.

Because it was developed as an analog to Ohm's law (current = electrical potential/resistance), this method is considered a resistance method. For meteorological applications, the ''current'' represents a flux, the ''potential'' is the gradient, and the ''resistance'' is the suitability of the medium for downgradient transfer. For a given gradient, a larger (smaller) resistance results in a smaller (larger) flux. Based on the Ohm's-law analogy, the following flux formulations are made:

$$u_*^2 = \frac{u(z_u) - u_g}{r_{\mathrm{aU}}} = \frac{u(z_u)}{r_{\mathrm{aU}}}, \tag{2}$$

$$H = \frac{T_g - T}{r_{\mathrm{aH}}}\rho c_p, \tag{3}$$

$$\mathrm{LE} = \frac{e_g - e}{r_{\mathrm{aL}}}\frac{\rho c_p}{\gamma}, \quad \text{and} \tag{4}$$

$$G = \frac{T_g - T_s}{r_{\mathrm{soil}}}\rho c_p + \text{storage term}, \tag{5}$$

where $-u_*^2$ is the momentum flux divided by the density of air, or the friction velocity squared; $u(z_u)$ is the mea-

sured wind speed at z_u (10 m); u_g is the surface (at $z = 0$) wind (zero); T_g and e_g are the surface temperature and vapor pressure at z_{0h}; T and e are the observed temperature and derived vapor pressure (from the observed relative humidity) at 1.5 m; r_{aU}, r_{aH}, and r_{aL} are the aerodynamic resistance to the momentum, sensible heat, and latent heat fluxes (s m^{-1}); T_s is the soil temperature at -10 cm; r_{soil} is the conductive resistance of the soil; ρ is the air density; and γ is the psychrometric constant. The storage term is necessary in (5) to account for the temperature changes in the top soil, which effectively reduce the transfer of heat through the soil. In this sense, the soil acts as a capacitor in the Ohm's-law analogy. The formulation for G will be outlined further in section 4b. Because momentum flux is always downward near the surface, the typical sign convention has been reversed in (2), with positive momentum fluxes representing downward transfer. Because r_{aH} and r_{aL} are usually of similar magnitude (Berkowicz and Prahm 1982), we will define and use one representative aerodynamic resistance r_a, where $r_a = r_{aH} = r_{aL}$.

Monteith (1965) showed that the latent heat flux could also be prescribed as:

$$\mathrm{LE} = \frac{e_{sg}(T_g) - e_g}{r_s}\frac{\rho c_p}{\gamma}, \tag{6}$$

where $e_{sg}(T_g)$ is the saturated vapor pressure at T_g, and r_s represents the total resistance of the vegetation to evapotranspiration. This equation describes the process of transferring water vapor to the atmosphere through transpiration from the vegetation. The formulation is based on the assumptions that the vapor pressure inside the stomata of the vegetation is saturated at the surface temperature, and that water vapor transfer occurs between the leaf and the drier air above. These assumptions are accurate in relatively steady atmospheric conditions, because the plant regulates its evaporation to maintain equilibrium with the overlying atmosphere (Rutter 1975).

The latent heat flux, which describes the total water-vapor transfer from the surface to the overlying atmosphere, occurs in two steps. The first is transpiration between the native vegetation and the adjacent air [(described by (6)]. This process is mainly a biophysical one, controlled by the plant reaction to external and internal processes. The second process is turbulent transfer between the newly moistened air adjacent to the surface and the atmosphere above [described by (4)], which is controlled by the near-surface wind speed and atmospheric stability. If it is assumed that no water vapor is lost through condensation on the vegetation, then either (4) or (6) can be used to calculate LE. Moisture transfer is represented as a series circuit, with LE representing the current (Fig. 3). Because the current remains constant throughout the circuit, we can set the rhs of (4) and (6) equal to each other. In doing so, e_g, which is not measured, can be eliminated from the system of equations.

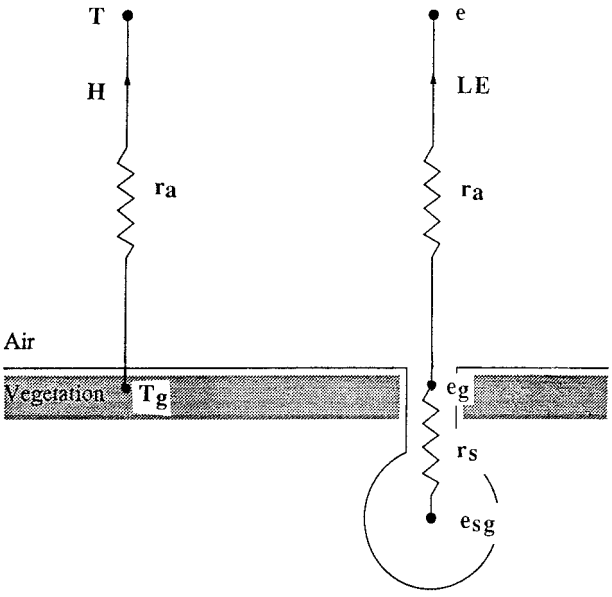

FIG. 3. Physical manifestation of Ohm's-law analogy (Lee 1992).

The following formulations can be derived for use with data from only one level, using (1), (3), (4), and (6):

$$\mathrm{LE} = \frac{(R_n - G)\Delta r_a \gamma^{-1} + [e_s(T) - e]\rho c_p \gamma^{-1}}{r_s + (1 + \Delta\gamma^{-1})r_a} \tag{7}$$

$$H = \frac{(R_n - G)(r_a + r_s) - [e_s(T) - e]\rho c_p \gamma^{-1}}{r_s + (1 + \Delta\gamma^{-1})r_a}. \tag{8}$$

Here, $e_s(T)$ is the saturation vapor pressure at T, and Δ is well approximated as the local change in saturation vapor pressure with respect to temperature ($\partial e_s/\partial T$) at T. For the PM approach to work, it must be assumed that Δ is constant between T_g and T. Because the PM method was developed for agricultural surfaces with little exposed soil, it is not expected to be as effective over bare soil. Most Mesonet sites are located in open fields of grass, however, which more closely resemble fields of crops than bare soil. Because the sites are fully vegetated, the method is expected to work reasonably well for this study.

The aerodynamic principles from which r_{aU} and r_a are derived are based on Monin–Obukhov similarity theory (Monin and Obukhov 1954), which depends on the assumption that the magnitude of the vertical gradient of any conserved quantity is a function of z/L, where z is the distance above ground and L is the Monin–Obukhov length:

$$L = -\frac{Tu_*^3}{gkH}\rho c_p, \tag{9}$$

where k is the von Kármán constant (0.4), and L is

negative for $H > 0$ (unstable surface layer) and is positive for $H < 0$ (stable surface layer).

Based on similarity theory, wind and temperature profiles can be related to surface fluxes as follows:

$$u(z) = \frac{u_*}{k}[\ln(z/z_{0m}) - \psi_m(z/L) + \psi_m(z_{0m}/L)] \quad (10)$$

$$T(z) = T_g + \frac{T_*}{k}[\ln(z/z_{0h}) - \psi_h(z/L) + \psi_h(z_{0h}/L)], \quad (11)$$

where T_* is the flux temperature scale, which is related to the sensible heat and momentum fluxes by

$$T_* = \frac{-H}{\rho c_p u_*}, \quad (12)$$

and where ψ_m and ψ_h are empirical stability correction functions (Paulson 1970; Dyer 1974):

$$\psi_m(z/L) = \ln\left[\left(\frac{1+x}{2}\right)^2\left(\frac{1+x^2}{2}\right)\right] - 2\tan^{-1}x + \frac{\pi}{2} \quad \text{for } L < 0$$

where $x = (1 - 16z/L)^{1/4}$, and

$$= -5z/L \quad \text{for } L > 0; \quad (13)$$

$$\psi_h(z/L) = 2\ln\left[\left(\frac{1+x^2}{2}\right)\right] \quad \text{for } L < 0, \quad \text{and}$$

$$= -5z/L \quad \text{for } L > 0. \quad (14)$$

The aerodynamic resistances can be obtained from (2) and (10):

$$r_{aU} = [\ln(z_u/z_{0m}) - \psi_m(z_u/L) + \psi_m(z_{0m}/L)]^2/[k^2 u(z_u)] \quad (15)$$

and (3), (11), and (12) (Berkowicz and Prahm 1982):

$$r_a = \frac{1}{k^2 u(z_u)}[\ln(z_u/z_{0h}) - \psi_m(z_u/L) + \psi_m(z_{0m}/L)] \times [\ln(z_t/z_{0h}) - \psi_h(z_t/L) + \psi_h(z_{0h}/L)], \quad (16)$$

where z_t is the height of the temperature measurement (1.5 m). In most circumstances, $r_{aU} < r_a$, because momentum transfer is enhanced by small pressure fluctuations in the turbulent wakes behind the roughness elements, unlike heat or moisture transfer (Garratt 1992).

The stability correction functions (13) and (14) ensure that r_{aU} and r_a are larger (smaller) in stable (unstable) conditions. It is also apparent from (16) that larger (smaller) values of $u(z_u)$, z_{0m}, and z_{0h} result in a smaller (larger) aerodynamic resistance, because both higher wind speeds and taller and/or rougher vegetation create more surface drag; increased drag causes more frictionally generated eddies and thus more vertical mixing (less resistance to vertical transfer).

The aerodynamic roughness length for momentum z_{0m} is that height at which surface drag reduces the wind speed to zero (Stull 1986). It is proportional to both the height and density of the native vegetation. Rougher surfaces (larger z_{0m}) are more strongly coupled to the atmosphere via turbulent transfer than are smooth surfaces. In fact, Lee (1992) noted that transpiration over grass-covered, moist surfaces has been found to be more significant than the evaporation over either wet soil or water, owing to the increase in turbulent transfer associated with the rougher surfaces, as well as the increased surface area available for evaporation and the ability to tap deeper soil water. Typical values of z_{0m} (Table 1) vary from 0.1–20 cm, according to the vegetation height, which may not be known accurately.

TABLE 1. Typical values of z_{0m} and vegetation height [adapted from Pielke (1984)].

Surface type	z_{0m} (cm)	Vegetation height (cm)
Soils	0.1–1.0	—
Short grass	0.3–1.0	2–10
Long grass	4–10	25–100
Crops	4–20	40–200

Because vegetation heights are not available operationally, simple assumptions about z_{0m} must be made. In this study, we assume that $z_{0m} = 0.01$ m and $h = 0.1$ m, which is typical for short grasses (Wieringa 1993). It is commonly assumed that the effective ''surface'' for heat and moisture (z_{0h}) is lower than z_{0m}. Garratt (1992) concluded that $z_{0h} = z_{0m}/e^2$ for practical applications over a wide range of surfaces, which is the formulation that is used in this study. To simplify the analysis, we assume that the wind between z_{0m} and the soil is calm, and that the moisture and temperature profiles between z_{0h} and the soil are constant.

3. Data

a. Oklahoma Mesonet

Measurements of air temperature and relative humidity are made at 1.5 m at all 116 sites with a Campbell Scientific, Inc./Vaisala, Inc., HMP35C dual probe. Readings, which are accurate on the average to 0.35°C and 3% relative humidity, are taken every 3 s and are averaged at 5-min intervals. Pressure is measured with a Vaisala, Inc., PTB 202 barometer at 12-s intervals, averaged over 5-min intervals; the readings are accurate to 0.4 mb.

The wind speed and direction are also measured at 10 m at 3-s intervals, with averaging every 5 min. An R. M. Young Company Model 5103 Wind Monitor, which has a starting threshold of 1 m s^{-1}, and an accuracy of 2% for speed and 3° for direction, is used. A LI-COR, Inc., 200SZ pyranometer measures downwelling shortwave radiation at a height of 1.8 m to within 5% and with a resolution of 0.23 W m^{-2}. The 5-min average is comprised of 100 3-s averages. Soil temperature is measured at 10 cm below the surface using a Fenwal Electronics soil thermistor. Samples are

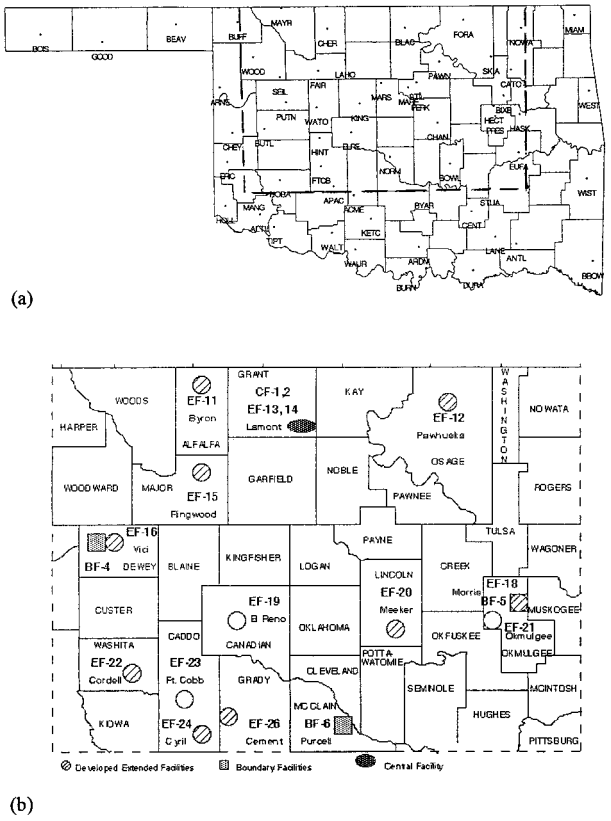

FIG. 4. (a) Locations of Mesonet soil moisture sensors. (b) Locations of ARM sites. EBBR sites are denoted with ''EF'' prefixes. Area in (b) is outlined in (a) with dashed lines.

taken at 30-s intervals, and are averaged over 15-min intervals; the readings are accurate to 0.5°C.

Campbell Scientific, Inc., (CSI) 229-L heat dissipation matric potential sensors have been installed at 60 of the Mesonet sites (Fig. 4a) at depths of 5, 25, 60, and 75 cm below the ground. These sensors are comprised of a thermocouple and a heater wire enclosed in a hypodermic needle. The needle is embedded in a cylindrical ceramic shield, whose porosity allows for equilibration with the surrounding soil (Reece 1996). An electric current is passed through the heater wire for 20 s, resulting in the production of heat from the resistance of the wire. This heat production is quantified as a rise in temperature within the sensor, as detected by the thermocouple. This temperature change can then be related to the matric (soil water) potential of the soil.

b. ARM

Observations from ARM were used to develop and to test the parameterizations in this study. Surface energy fluxes are measured at 14 energy balance Bowen ratio (EBBR) sites across Oklahoma (Fig. 4b), along with air temperature, vapor pressure, and wind speed. Two 13-min averages of 30-s samples were then averaged to get 30-min values.

4. Methodology

a. Net radiation (R_n)

The net radiation received at the surface is composed of four components:

$$R_n = \mathrm{SW}_d - \mathrm{SW}_u + \mathrm{LW}_d - \mathrm{LW}_u, \qquad (17)$$

where SW and LW represent broadband shortwave (0.15–3.0 μm) and broadband longwave radiation (3.0–100.0 μm), respectively. The subscripts u and d refer to upwelling and downwelling, respectively. Of these four components, only SW_d is measured at the Mesonet sites.

1) DOWNWELLING SHORTWAVE RADIATION (SW_d)

The pyranometer detects incoming direct shortwave radiation from the entire upward-looking hemisphere at wavelengths from 0.4–1.1 μm; the peak spectral response of the instrument is at 0.95 μm. The pyranometers are calibrated against a higher quality sensor (one that measures radiation at all solar wavelengths) before being installed in the field. This calibration compensates for the wavelengths that the pyranometer cannot detect.

2) UPWELLING SHORTWAVE RADIATION (SW_u)

The upwelling shortwave radiation is parameterized as follows:

$$\mathrm{SW}_u = \alpha \mathrm{SW}_d, \qquad (18)$$

where α is the surface albedo. Albedos vary both diurnally and annually. For flat terrain and constant soil moisture, the diurnal cycle is characterized by higher values in the early morning and late afternoon, with the smallest values around solar noon.

The annual cycle of albedo is mainly a function of climatological soil wetness, and the color and state of the natural vegetation. Wetter soils are darker and have lower albedos. In Oklahoma, soil wetness is greatest in late spring, concurrent with the rainfall maximum. The color of the vegetation is also important. Active vegetation (green) has a lower albedo than dormant vegetation (light brown or yellow). In general, Oklahoma is most ''green'' in late spring (Loveland et al. 1991), concurrent with its rainfall maximum. The combination of wet soil and the color of the vegetation produces a sinusoidal variation in albedo.

To parameterize the albedo more effectively, six years of SW_u and SW_d observations from a Norman experimental site were acquired (C. Duchon 1996, personal communication) and averaged to produce a ''climatological'' annual albedo variation (Fig. 5). Individual days with missing data or with abnormally high albedos (from snow cover) were not included in the average. From a Fourier analysis of the averaged time series it was found that the annual cycle (harmonic 1) accounted for 69% of the total variance of the time series. Other

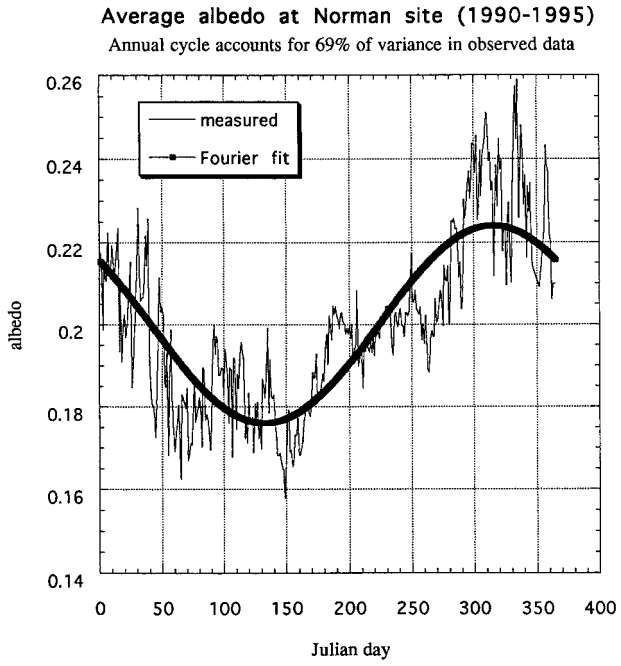

FIG. 5. Annual albedo variation at Norman radiation site.

individual harmonics accounted for no more than 5% of the total variance. Thus, it seems reasonable to model the annual albedo variation with a sine wave. The range of albedos corresponds well to the 0.18–0.25 range specified by Oke (1987) for most crops and natural vegetation.

The amplitude and phase of the modeled albedo variation are left constant for all locations, while the mean albedo varies across the state in order to represent the climatological variation in rainfall and greenness. To specify the mean at each location, a monthly mean albedo chart derived from satellite estimates from the Global Energy and Water Experiment (GEWEX) Continental-Scale International Project (GCIP; Leese 1993) from April 1996 was used (not shown).

3) DOWNWELLING LONGWAVE RADIATION (LW_d)

The downwelling longwave radiation (LW_d) is calculated from observed values of temperature, humidity, pressure, and solar radiation, using a method outlined in detail in Crawford and Duchon (1999). Because solar radiation observations are used as a proxy for cloudiness, the estimates of LW_d (and thus R_n) are only useful in the daytime. Because of this limitation, the surface energy budget model is itself also limited to daytime use.

4) LONGWAVE RADIATION (LW_u)

Outgoing longwave radiation (LW_u) is a function of the temperature T_g and emissivity ε_g of the surface:

$$LW_u = \varepsilon_g \sigma T_g^4. \tag{19}$$

Surface emissivities at all sites are set in the model to 0.98, which is representative of natural land surfaces in Oklahoma (Humes et al. 1994). Here, T_g is set to the temperature at z_{0h} and is calculated by rearranging (3):

$$T_g = T + r_a H/\rho c_p. \tag{20}$$

The estimated value of H from the previous 5-min observation is used in (20) to calculate T_g.

b. Ground heat flux (G)

If it is assumed that there is no horizontal conduction of heat in the first 5 cm of soil, then the rate of change of temperature within that soil layer is determined by the heat-flux gradient between the top and bottom of the layer (Garratt 1992):

$$c_s \frac{\partial T_{2.5}}{\partial t} = \frac{\partial G}{\partial z} = \frac{G - G_5}{0.05}, \tag{21}$$

where c_s is the heat capacity per unit volume of soil and T_5 is the 5-cm soil temperature, which is used to represent the layer-averaged temperature. Here, G represents the soil heat flux at the surface (ground heat flux), and G_5 represents the 5-cm soil heat flux:

$$G_5 = k_{\mathrm{Hs}} c_s \frac{\partial T_s}{\partial z} = \lambda \frac{T_g - T_{10}}{0.1}, \tag{22}$$

where k_{Hs} and λ are the thermal diffusivity and thermal conductivity of the soil, T_s represents the soil temperature, and T_{10} is the soil temperature at a depth of 10 cm. Combining (21) and (22) and making the assumption $\partial T_5/\partial t = \partial T_{2.5}/\partial t$, leads to

$$G = 0.05 c_s \frac{\partial T_5}{\partial t} + \lambda \frac{T_g - T_{10}}{0.1}. \tag{23}$$

The first term on the rhs of (23) is referred to as the storage term, because it represents the energy that is ''stored'' in the top soil as heat. The soil-moisture sensors measure T_5 and the soil-temperature sensors measure T_{10}. Since T_5 is measured only every 30 min, linear interpolation is used to estimate values at 5-min intervals. The method for estimating λ and c_s will be outlined subsequently. The second term is the flux term, because it represents the transfer of energy through the soil. The flux term is typically 5–10 times larger than the storage term (C. Marshall 1997, personal communication).

1) CALCULATING THERMAL CONDUCTIVITY

A large (small) temperature rise in the sensor implies that the soil cannot effectively conduct the heat away from the sensor because of low (high) λ. It is well known that low (high) λ is associated with dry (wet) soil.

Average temperature changes were compiled from 20 measurements made with each of the 221 available

229-L probes, in both ''dry'' and ''wet'' soils. Since the range of sensor responses for a given soil wetness is greater than 1°C, adjustments were made to each of the sensor responses to normalize them. Sensors then were tested against known values of soil water potential (ψ) in order to establish the relationship between sensor response and potential. The soil water potential, the work required to extract water from the soil against surface tension, is expressed as a negative quantity in terms of work per unit mass of water. Multiplied by the density of water ($\sim$1000 kg m^{-3}), ψ can be expressed as a pressure. Larger absolute values imply drier soil, since it takes more work to extract the remaining water. Regression analysis yields the following (Basara et al. 1998):

$$\psi = \frac{1}{a}\left[\left(\frac{dT_w - dT_d}{dT_{\text{ref}} - dT_d}\right) - 0.9\right]^{1/n}, \tag{24}$$

where $a = -0.01$ kPa^{-1}, $dT_w = 1.45$°C, $dT_d = 4.0$°C, $n = 0.77$, and

$$dT_{\text{ref}} = b_1\Delta T + b_2, \tag{25}$$

where b_1 and b_2 are the two aforementioned calibration coefficients that are unique to each sensor, and ΔT is the temperature change.

The thermal conductivity is calculated from ψ. Al Nakshabandi and Kohnke (1965) concluded that this relationship is independent of soil type. Reece (1996) calibrated six 229-L sensors against standard potentials and found that the inverse of the thermal conductivity was linearly related to the logarithm of the potential:

$$\lambda^{-1} = 0.134 + 0.529\ \ln(-\psi). \tag{26}$$

Because the 229-L sensors are also installed at the Mesonet sites, this relationship is used in this study.

2) CALCULATING HEAT CAPACITY

In this study, c_s is calculated using the following equation (de Vries 1963):

$$c_s = 1.93V_m + 2.51V_{\text{om}} + 4.19\eta, \tag{27}$$

where V_m and V_{om} represent the fractional volume of solids and organic matter in the soil, respectively, and η is the fractional volume of water in the soil (volumetric water content). In our model, we approximate $V_m = 0.5$ and $V_{\text{om}} = 0$. To calculate η, the following calibration equation relating η to ψ was employed (K. Fisher 1997, personal communication):

$$\eta = \eta_r + \frac{\eta_s - \eta_r}{\{1 + [\alpha(-\psi/100)]^n\}^{(1-1/n)}}, \tag{28}$$

where η_r and η_s are the residual and saturated water content, and α and n are empirical constants. Each soil moisture sensor has unique values of η_r, η_s, α, and n, which are representative of the soil at a given site.

c. *Latent heat flux (*LE*)*

Evapotranspiration from the surface is due primarily to transpiration from vegetated surfaces (except for within 1–2 days immediately following precipitation events, when evaporation is dominant). Pores on the surface of the vegetation (stomata) open during the daytime in response to sunlight in order to take in carbon dioxide and to begin the process of photosynthesis. In doing so, the watery interior of the plant is exposed, allowing transpiration to occur. The latent heat flux, then, which describes the vertical transfer of water vapor from the surface (vegetation and soil) to the overlying atmosphere, can be calculated using the PM formula (7).

The two resistance terms in the denominator of (7) strongly modulate the magnitude of LE. Because more turbulent vertical mixing (and thus more evaporation) occurs with stronger winds (smaller r_a), one would expect LE to be inversely proportional to r_a; similar logic applies to r_s. If plant stomata are closed (high r_s), LE will be reduced. Mesonet observations provide the humidity deficit term directly; parameterizations for the $(R_n - G)$ and r_a have been described in sections 4a and 4b, respectively. Previous formulations for r_s have been developed [see Niyogi and Raman (1997) for a review] that are dependent upon vegetation properties and numerous empirical coefficients. For use in this study, a simple model relating r_s to available meteorological data is needed to estimate LE.

A second-order approach must be used to model r_s, because routine observations of stomatal behavior are not available. Retrievals of r_s can be obtained by rearranging the PM equation as follows:

$$r_s = \frac{(R_n - G)\Delta\gamma^{-1} + \{e_s[T(z_t)] - e(z_t)\}\rho c_p\gamma^{-1} - (1 + \Delta\gamma^{-1})r_a\text{LE}}{\text{LE}}. \tag{29}$$

Observations of R_n and G, as well as H and LE (computed using the Bowen-ratio method) are provided at many of the ARM sites. The data at these sites are sufficient to account for all the terms on the rhs of (29), except for r_a. To estimate r_a, the Monin–Obukhov length L is systematically varied from $-10\,000$ (10 000) m to 0 for positive (negative) observed H until the calculated H [from inverting (9)] converges to the observed H.

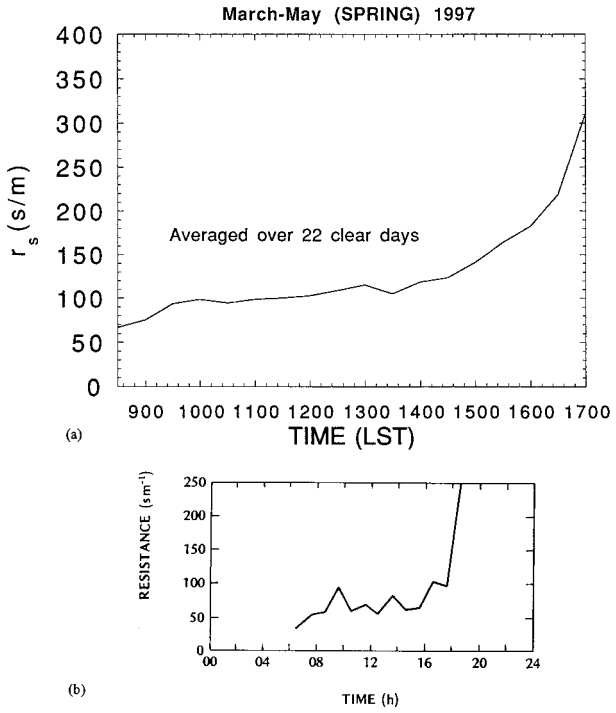

FIG. 6. (a) Average calculated r_s for Mar–May 1997 at the Lamont CF from 0830–1700 LST. Average is composed of 22 clear days. (b) Surface resistance of a barley field at Rothamsted, England, on 23 Jul 1963.

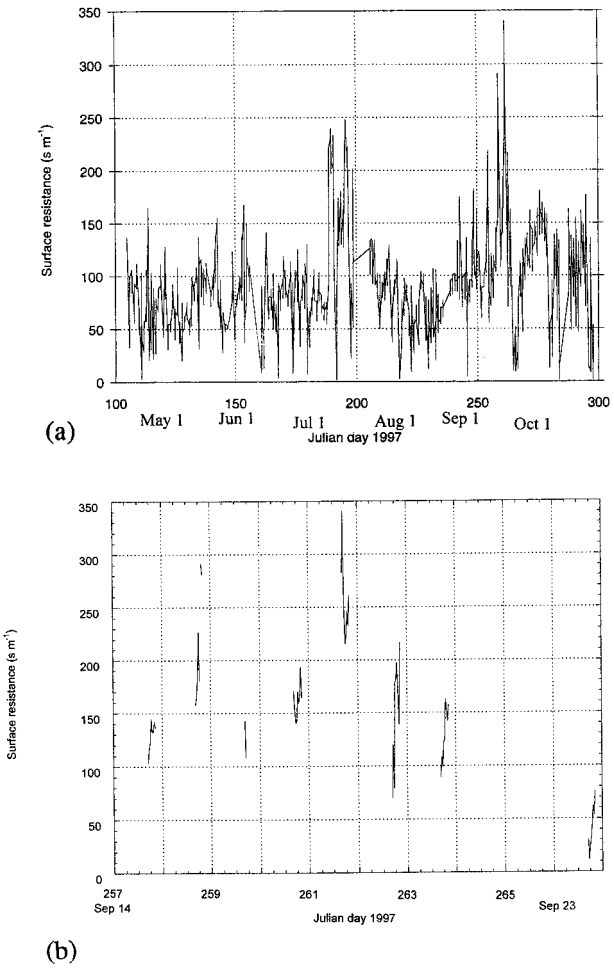

FIG. 7. (a) Surface resistance time series at Lamont for yeardays 105–298. (b) Surface resistance time series at Lamont for yeardays 257–266.

Then r_a is calculated from (16), followed by the calculation of r_s from (29). To test this method for extracting r_s, one full year of data (July 1996–June 1997) from the ARM Central Facility (CF) at Lamont were analyzed at half-hourly intervals. To reduce noise in the dataset, only clear days were examined. These days were qualitatively selected by viewing the observed SW_d data. During the spring, a moderate 1–2 h rise of the seasonally averaged r_s in the morning (Fig. 6a) is probably associated with the evaporation of dew; r_s increases more slowly throughout the course of the midday hours, because water lost through transpiration is replenished by water from deeper soil layers. As the magnitude of solar radiation decreases in the late afternoon, the plant stomata begin to close as a self-preservation mechanism to reduce excessive water loss (because it cannot photosynthesize anymore), resulting in a rapid increase in r_s. The character of the diurnal cycle of these derived values compares favorably to directly observed values over a barley crop in England [Fig. 6b; Oke (1987, p. 135)]. The character of the summer and fall time series from the ARM site (not shown) is similar to the spring time series.

Next, the retrieved values of r_s were compared with the more commonly observed atmospheric variables from the ARM site in Lamont. The retrieved values of r_s for one growing season (22 April–24 October 1997) were correlated with the following variables: vapor pressure deficit (VPD), soil water potential (SWP), SW_d, and T. The SWP observations were taken at Blackwell (BLAC), which is the nearest mesonet site (~20 km away). Unfortunately, the soil-moisture measurements at Lamont itself were not good enough for this study because of large blocks of missing or spurious data (K. Fisher 1997, personal communication). The correlations were computed at 30-min intervals from 1000–1400 LST; after bad data had been eliminated, 1448 point comparisons were available for analysis. During periods of small H (large L), the method used to evaluate (29) would often fail since the observed L would be well out of the range of iteration. Because of this, the r_s analysis is limited to midday hours (1000–1400 LST).

Between spring and early summer, there is little change in the mean value of r_s at Lamont (Fig. 7a). Around yearday 190, there is a sharp increase in r_s, which is associated with an extended spell of dry weather. Summer rains then reduce r_s back to spring levels. In late summer, r_s increases sharply, along with a cor-

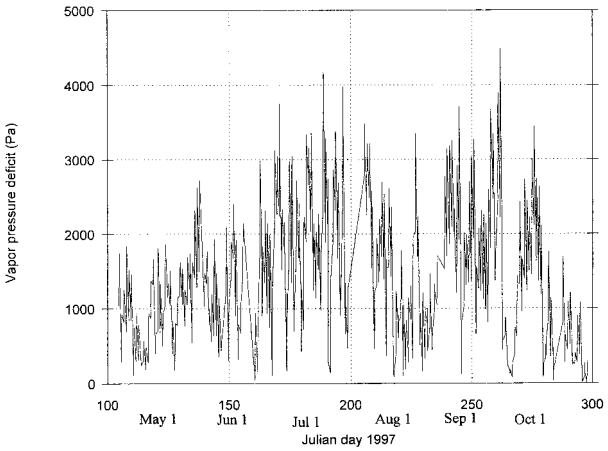

FIG. 8. Vapor pressure deficit time series at Lamont.

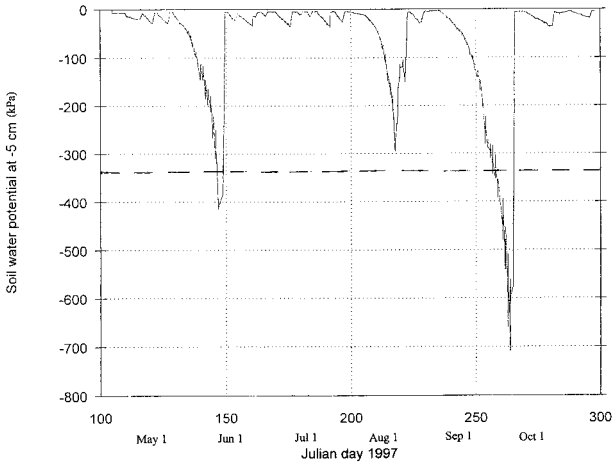

FIG. 9. Soil-water potential time series at BLAC. Dashed line represents wilting-point value of −330 kPa.

responding increase in diurnal variability (Fig. 7b). In general, the larger values of r_s occur throughout the late summer and early fall. VPD increases significantly from spring to early fall as well, with more humid conditions noted in early August, and again in portions of September and October (Fig. 8). Because the saturation vapor pressure increases exponentially with temperature (while the observed vapor pressure does not), VPD should be expected to be larger in the warmer months of the year.

The temperature and solar radiation (not shown) both peak in summer as expected. There are only three periods of significant drying of the soil—in mid-May, early August, and late September (Fig. 9). It is surprising that there is no significant correlation between SWP and r_s, except for the driest period in late September. Lee and Pielke (1992) noted that ''when the soil–water content is greater than the field capacity, the soil should behave very close to the saturated soil.'' The soil field capacity is defined as the amount of moisture a thoroughly wetted soil retains after two days of drying (Marshall et al. 1996, p. 11). It is commonly assumed to be near −330 kPa, but can vary greatly with soil texture (Clapp and Hornberger 1978). The resistance r_s was relatively independent of SWP because the soil was drier than −330 kPa only twice throughout the period of interest (Fig. 9).

Of the four observed variables, r_s is most strongly correlated with VPD (Fig. 10). VPD is therefore considered the most significant, or first-order, contributor to r_s:

$$r_{s1} = \text{VPD}/20, \tag{30}$$

where r_{s1} represents the first-order contribution to r_s. Both SW_d and T were also well correlated with r_s, and SW_d correlated slightly more significantly with r_s (the second-order contributor, r_{s2}). Again, a linear relationship was determined:

$$r_{s2} = \begin{cases} 85 - 0.1(\text{SW}_d) & \text{for VPD} > 500 \text{ Pa} \\ 0 & \text{for VPD} < 500 \text{ Pa;} \end{cases} \tag{31}$$

T was the third-order contributor (r_{s3}):

$$r_{s3} = \begin{cases} -10(T - 30) & \text{for } T > 30°\text{C} \\ 0 & \text{for } T < 30°\text{C;} \end{cases} \tag{32}$$

One final relationship is constructed (the fourth-order contributor, r_{s4}):

$$r_{s4} = \begin{cases} -2(\text{SWP} + 330)/5 & \text{for SWP} < -330 \text{ kPa} \\ 0 & \text{for SWP} > -330 \text{ kPa.} \end{cases} \tag{33}$$

The r_s model has a simple form:

$$r_{\text{sw}} = \sum_{i=1}^{4} r_{si}, \tag{34}$$

where r_{sw} represents the r_s parameterization in western Oklahoma. Because of uncertainties in both observations and the underlying theory, however, the modeled values of r_s have a mean bias error (MBE) of 5.9 s m^{-1} and an rmse of 30.0 s m^{-1} with respect to the retrieved values. Because a typical value of r_s is 100 s m^{-1}, the modeled values of r_s are accurate to within approximately 30%.

Preliminary calculations suggest that use of this r_s parameterization is responsible for significant overestimates of H (because r_s is too large) in the eastern part of Oklahoma. Satellite estimates of greenness (Loveland et al. 1991) and statistical analyses of rainfall patterns (Richman and Lamb 1985) suggest that Oklahoma can be divided crudely into two land-use types (''green'' in eastern Oklahoma, ''brown'' in western Oklahoma). It was therefore determined that a second parameterization should be developed for eastern Oklahoma sites. Similar

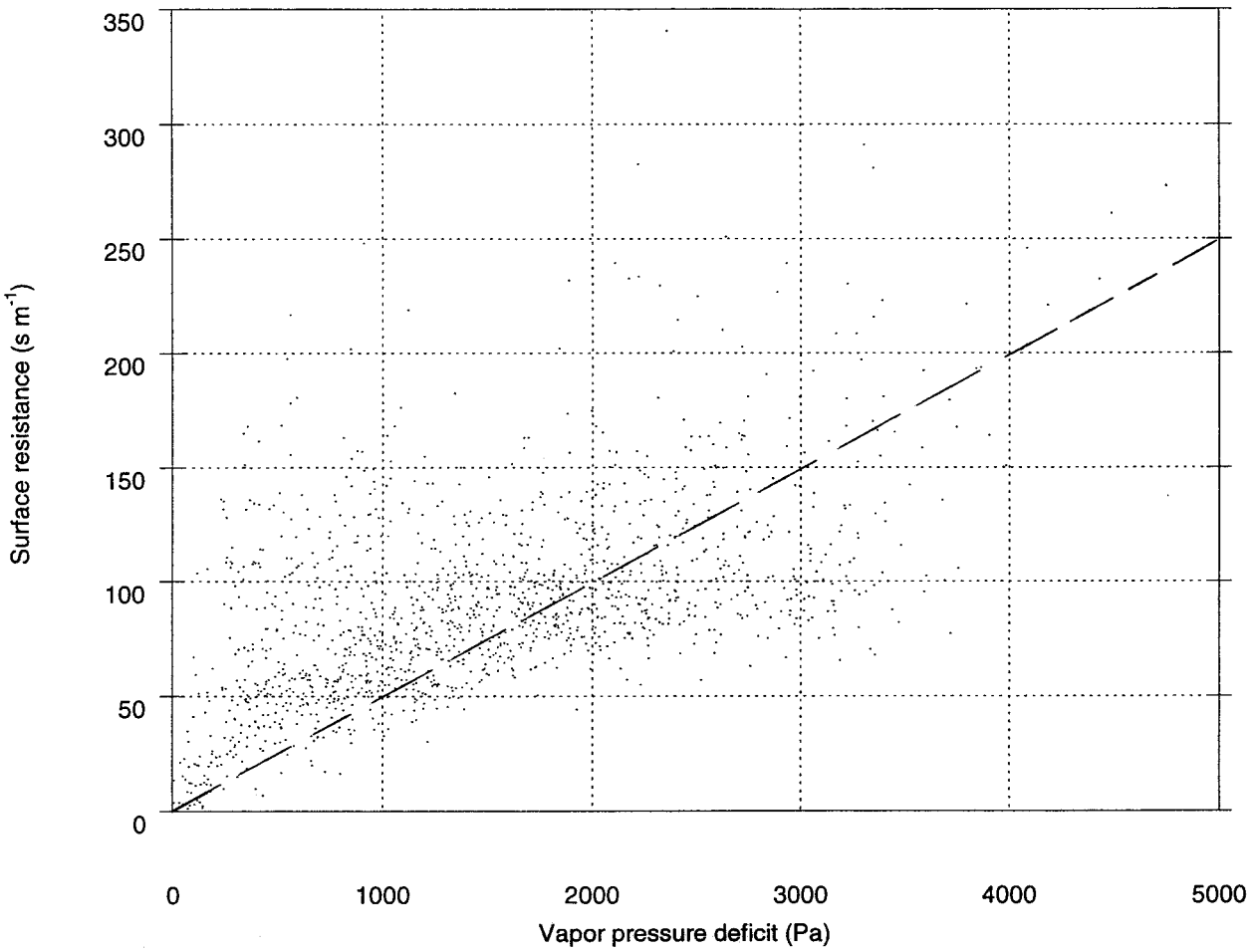

FIG. 10. Scatterplot of surface resistance and vapor-pressure deficit at Lamont. Dashed line represents relationship described in (31).

correlation analyses were performed using the r_s values at the Pawhuska (refer to Fig. 4b for location) ARM site (Fig. 11) for VPD, T, SW_d, and SWP, with the following results:

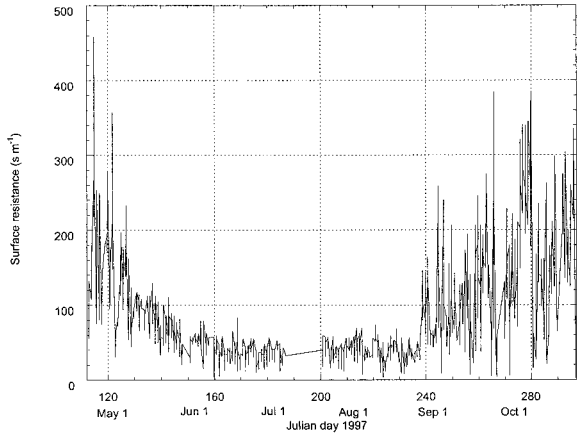

FIG. 11. Time series of r_s at Pawhuska ARM site during the growing season of 1997.

$$r_{se} = \sum_{i=1}^{5} r_{si}. \quad (35)$$

Here, r_{s5} represents the sinusoidal variation in the r_s values:

$$r_{s5} = \{80 - 115 \sin[(\pi(\text{day} - 110)/170]\}, \quad (36)$$

where day is the yearday. This sinusoidal variation is the only difference between the r_s parameterizations at Pawhuska and Lamont. The reason for this dependence is unknown but probably is caused by differing vegetation types and the character of their associated growing cycles. Modeled values of r_s at Pawhuska have an MBE of 0.6 s m^{-1} and an rmse of 44.1 s m^{-1}, which are slightly higher than the MBE and rmse of the Lamont comparisons. It is important to note that the ARM error statistics corresponding to the surface resistance formulations in (34) and (35) may not necessarily represent the magnitude of the r_s errors at the Mesonet sites. Because the errors at the Mesonet sites cannot be evaluated without measurements of latent heat flux, however, the ARM results must be used instead.

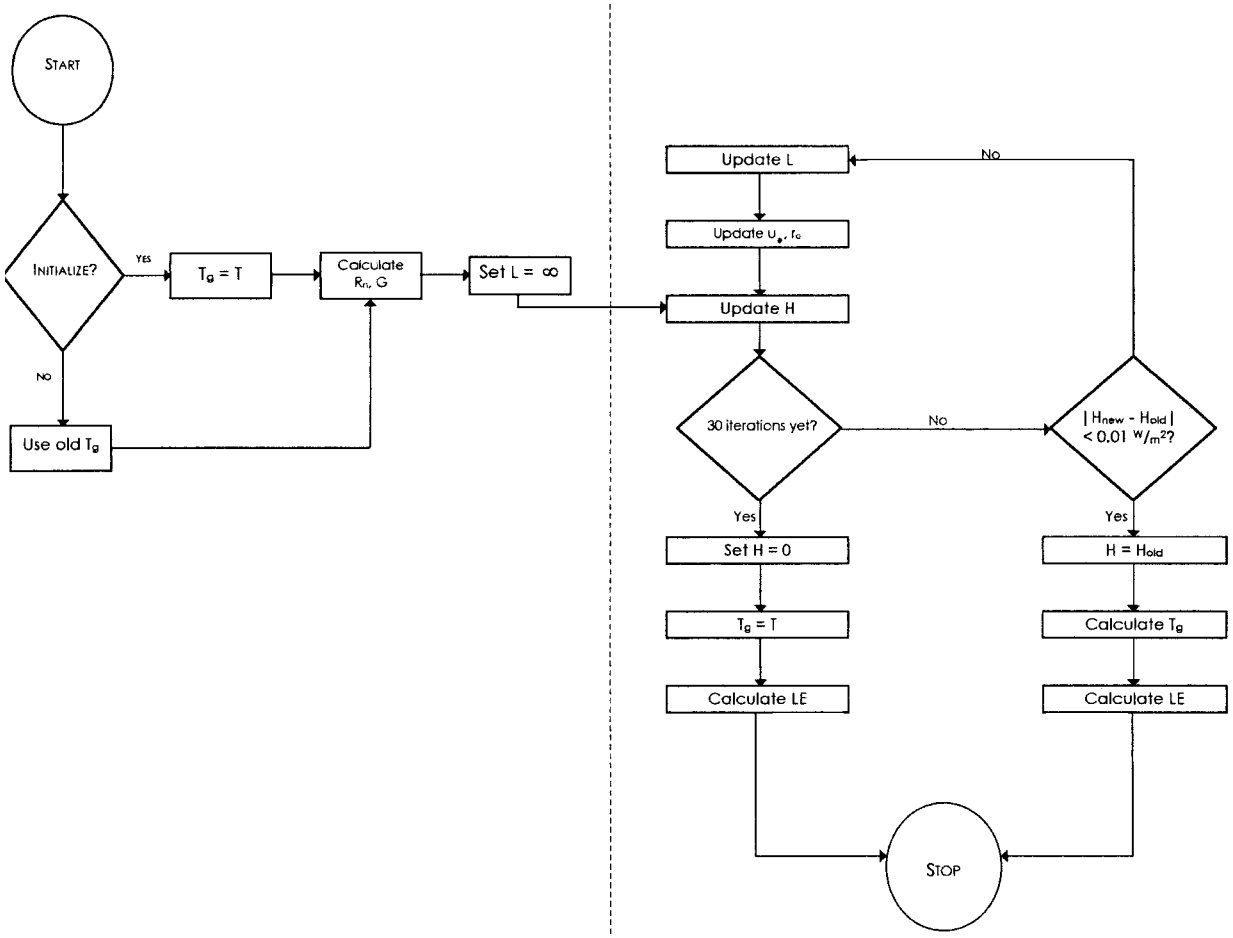

FIG. 12. Flow chart describing the computational process used to calculate surface fluxes at each 5-min interval.

d. Sensible heat flux (H)

Once the latent heat flux is specified through a partitioning of the available energy ($R_n - G$) using the PM equation, the sensible heat flux becomes a residual in the surface energy budget (8). To initialize the model in the first time step, T_g is set equal to T. Because the aerodynamic resistance r_a is a function of L, an iterative procedure must be employed to solve for H (Fig. 12). In this procedure, L is set initially to a very large value (representing a neutral surface layer), and values for r_a [from (16)] and H are calculated. A new value of L is calculated from H [from (9)], and the process continues through 30 iterations until H converges to within 0.01 W m^{-2}. If H has not converged after 30 iterations, H is set to zero, and T_g is set to T. If H has converged, T_g then can be obtained using the calculated sensible heat flux in (20). This process is repeated at each 5-min interval during the day.

5. Results and discussion

To test the accuracy of the energy-budget model, Mesonet data from July (1997) were used, because significant synoptic weather fluctuations are infrequent during the summer; thus there is a relatively undisturbed environment in which to compare the modeled and observed fluxes. Because the parameterization for R_n is valid only in the daytime, the estimates of H, LE, and G are useful only during the day as well.

a. Net radiation (R_n)

Observations of R_n taken at 15-min intervals at five Mesonet stations were used to verify the R_n parameterization. Three 5-min estimates of R_n were averaged and compared with the 15-min average observed value. All of the daytime data (measured $R_n > 0$) from July 1997 were analyzed at each of the five stations (Table 2).

The average MBE for all five sites is negligible (-5.1 W m^{-2}); the average rmse is only 21.6 W m^{-2}, or about 5% of a typical value of R_n. Even though R_n is computed from four separate terms, three of which are parameterized, these rmse values are very satisfactory. The y intercepts of the regression lines (e.g., see Fig. 13 for the GOOD site) are all below 15 W m^{-2} (where 0 W m^{-2} is a perfect fit) and the slopes are between 0.9 and

TABLE 2. MBE and rmse of the R_n parameterization applied at the five enhanced Mesonet sites at 15-min intervals during the daytime in Jul 1997.

Site	MBE (W m^{-2})	Rmse (W m^{-2})
APAC	−6.2	21.8
GOOD	−17.0	25.5
MARE	−8.6	24.3
NORM	1.0	18.0
WIST	−6.9	18.4

1.0 (where 1.0 is a perfect fit). It is apparent that the newly developed R_n parameterization performs very well across the entire state. The ability to model R_n accurately is crucial, because it represents the input to the land–atmosphere system. Inaccurate estimates of R_n provide little chance to represent H or LE accurately.

b. Ground heat flux (G)

There are two ARM sites that are nearly collocated (within 100 m) with Mesonet sites (El Reno and Pawhuska, respectively). The ARM method for estimating G involves measurements at five different locations near the site. The object is to sample the area well and then

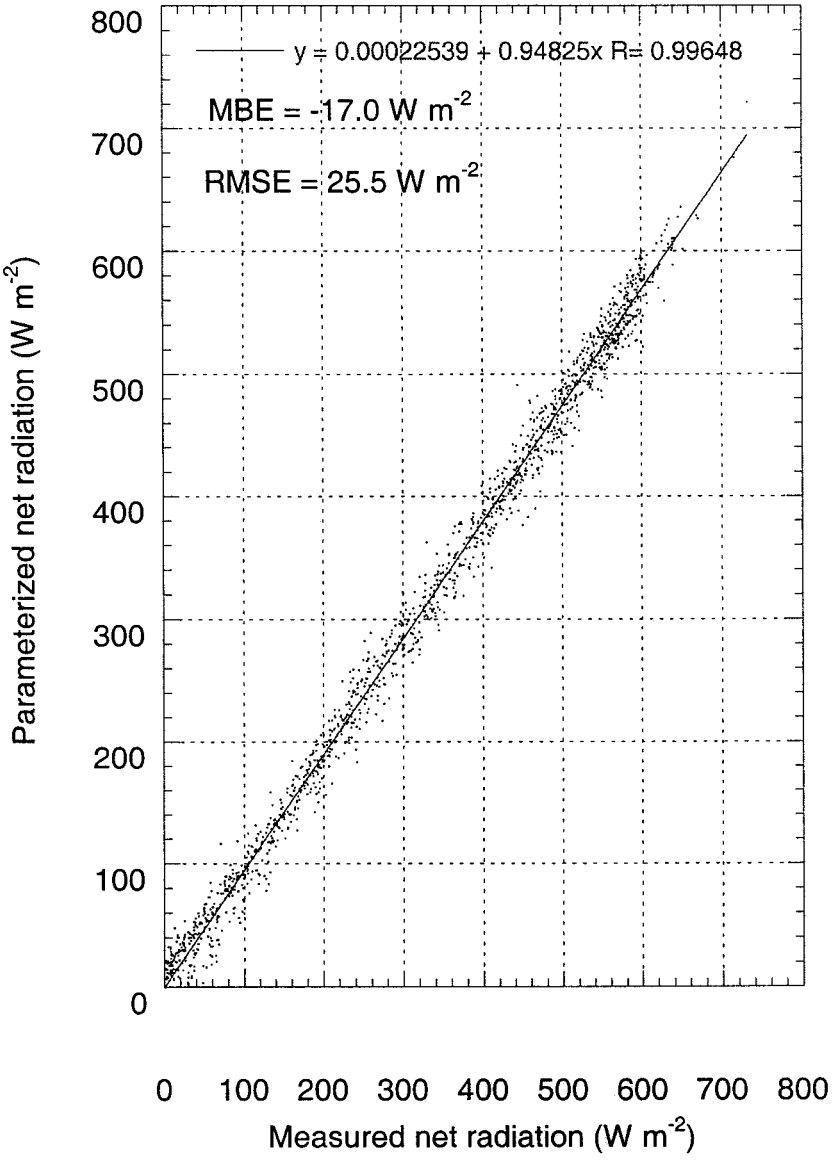

FIG. 13. Comparison of observed and calculated R_n at 15-min intervals from the daylight hours ($R_n > 0$) of Jul 1997 at GOOD. The solid line represents the results of the linear regression. The R is the correlation coefficient. Mean bias errors and rmses are also given.

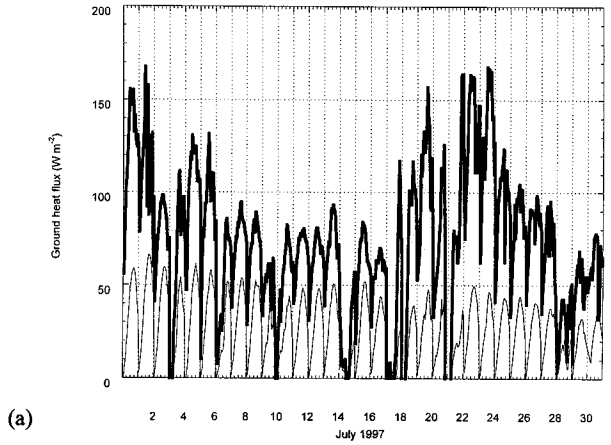

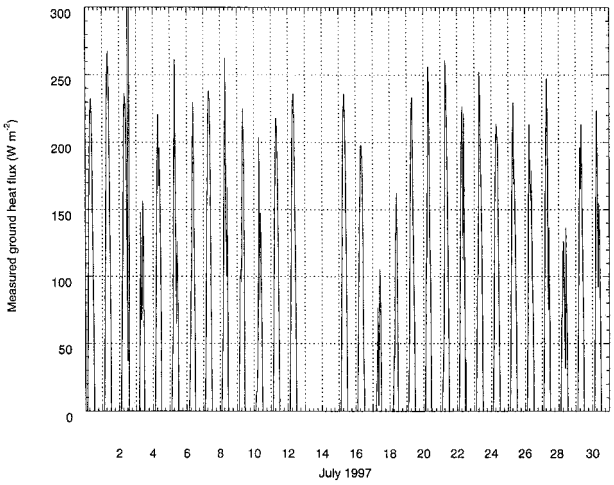

FIG. 15. Measured G at the NORM site during Jul 1997.

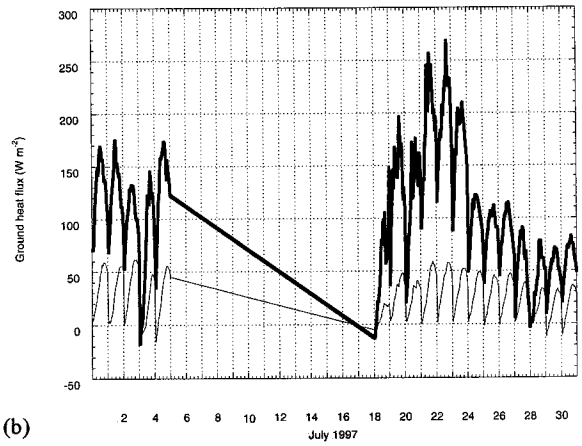

FIG. 14. Time series of observed (thin) and modeled (thick) G at (a) El Reno ARM site and El Reno Mesonet site, respectively, and (b) at the Pawhuska ARM site and Foraker Mesonet site. Data were missing from 6 to 18 Jul.

take the average of all the measurements to get a representative value. Thirty-min averaged values of G from the ARM sites were compared from 0800–1600 LST with the parameterization of G using the Mesonet data at the 5-min observation corresponding to the end of the 30-min averaging period. At El Reno (Fig. 14a), the observed values generally peaked around 50 W m^{-2}; there was only a small general decrease during the month. The parameterized values, however, ranged from about 10% larger to up to three times as large as the observed values. Peak values varied significantly throughout the month, ranging from approximately 50–170 W m^{-2}. The Pawhuska–Foraker comparisons (Fig. 14b) are similar.

The parameterized values are too large, probably because the height of the vegetation at the ARM sites is greatly underestimated. The native vegetation at all the Mesonet sites was assumed to be 10-cm high, an order of magnitude shorter than the 1–2 m heights at the ARM sites. Taller vegetation transfers more of the net radiation into the turbulent fluxes (H and LE) because the surface roughness is greatly increased and the aerodynamic resistance is decreased. Tall vegetation, furthermore, more effectively shades the underlying soil, keeping it cooler, so that smaller values of G are observed. At sites with shorter grasses, such as NORM, however, the observed magnitude of G is much larger (Fig. 15). At NORM, grass was approximately 15–30-cm high during July 1997 (C. Marshall 1998, personal communication), so that the soil warmed more readily. The range in variation of G from El Reno to Norman is similar to that found by Gao et al. (1998) in an examination of all of the ARM sites (their Fig. 2d).

Increasing the height of the vegetation by an order of magnitude affects the modeled ground heat flux [(16), (20), (23)]. Increasing the roughness length for momentum from 0.01 to 0.1 m (and corresponding changes in the roughness length for heat) decreases T_g by only $\sim$0.2 K and the ground heat flux by $\sim$2 W m^{-2}. This analysis is valid only if the temperature remains constant in the region between z_{0h} and the ground, however. Observations suggest that the temperature instead may decrease significantly beneath z_{0h} (Oke 1987, p. 138). If this were the case, the actual ground temperature would be significantly cooler under tall grass than under short grass (Fig. 16). A difference in ground temperature (ΔT) of 5 K corresponds to an $\sim$50 W m^{-2} difference in G, which would account for most of the difference in observed ground heat flux between that at the El Reno ARM site and that at the NORM Mesonet site. The exact magnitude of the slope of the temperature profile beneath z_{0h} is unknown, however, so only qualitative conclusions can be drawn.

It is apparent, though, that the instantaneous vegetation height must be known at a given location to estimate G accurately, because errors in vegetation height

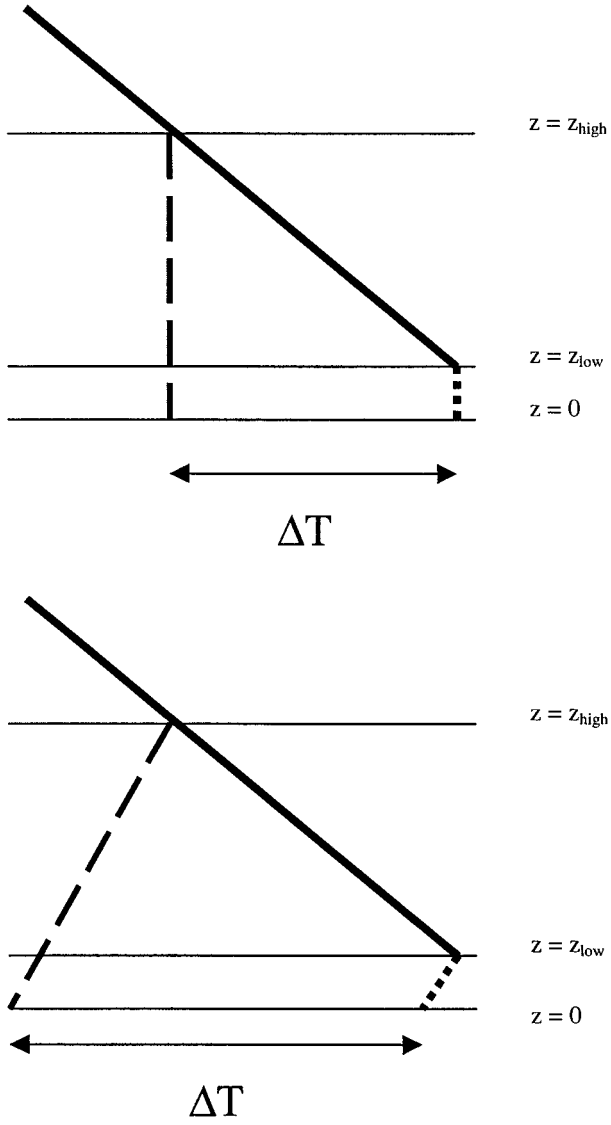

FIG. 16. Idealized near-surface temperature profiles for small ($z = z_{low}$) and large ($z = z_{high}$) roughness lengths. The thick solid line represents the background temperature profile. The long-dashed (short-dashed) line represents the temperature profile beneath the height of the roughness length for large (small) roughness length. The top (bottom) figure depicts constant (decreasing) temperature beneath the height of the roughness length. Here, ΔT is the expected ground temperature difference between the large and small roughness lengths. Note that ΔT is much larger in the case of decreasing temperature beneath the height of the roughness length (bottom figure).

will significantly outweigh errors in the observations and in the parameterization of the soil thermal conductivity and heat capacity. Because these data are not available for this study, the simple assumption of constant vegetation height will have to suffice.

c. *Latent heat flux (*LE*)*

Once R_n and G are calculated, the quantity $(R_n - G)$ is partitioned into LE and H [(1)]. First, LE is calculated using the Penman–Monteith Eq. (7); then H is determined as a residual ($H = R_n - G -$ LE). Unfortunately, no measurements of LE are available at the Mesonet sites, and the Bowen-ratio instrumentation during July 1997 at the two ARM sites collocated with Mesonet sites (El Reno and Pawhuska) had significant problems. The modeled latent heat fluxes therefore could not be verified.

d. *Sensible heat flux (H)*

Brotzge and Crawford (2000, hereinafter BC) equipped nine Mesonet sites with matching temperature and wind sensors at two levels. Using a variation of an aerodynamic method developed by Halliwell and Rouse (1989), BC calculated sensible heat fluxes at the Foraker site and compared them with the ARM values at the Pawhuska site for a 10-day period in May 1997. The comparisons were very good with the exception of days with light winds, when the afternoon sensible heat fluxes were overestimated by 50–150 W m^{-2}, because the instrumentation was radiatively heated. Because the results of the BC method otherwise compared favorably to the ARM data, we use their estimates as verification for evaluating the new sensible heat flux estimates.

Of the nine specially equipped Mesonet sites, only five have soil-moisture sensors, which are necessary to evaluate the sensible heat flux estimates using our model. At three of these five sites, data during the period had significant errors. The two remaining sites available for verification are Beaver (BEAV) and Nowata (NOWA). Because BEAV is located in the semiarid eastern panhandle and NOWA is located in the greener, humid eastern part of the state, data from these sites provide a good test of the versatility of our method.

Wind speed data from each site were analyzed to eliminate days when the BC method does not work because the winds are too light ($<$4 m s^{-1}). Also, cases from days with cloud cover were eliminated to reduce the amount of noise in the comparisons. During partly cloudy periods, rapid fluctuations in downwelling solar radiation will result in unrepresentative comparisons. The BC sensible heat flux estimates are taken based on the temperature gradient between 1.5 and 9 m, and the model uses the temperature gradient between z_{0h} and 1.5 m. During periods of rapid fluctuation in net radiation, these two flux estimates may be much different because of microscale temperature fluctuations. Because of this fact, we decided that using the clear days was the most effective way to test the model. There were five remaining ''golden'' days at BEAV during July 1997; for these days, the modeled values of H were compared with the BC value of H.

On 2 July (Fig. 17a), the phases of the modeled and BC time series of H are similar, and the magnitudes are within 80 W m^{-2} of each other, showing particularly good agreement during the midday hours. The next day (Fig. 17b), the model performed poorly in the morning

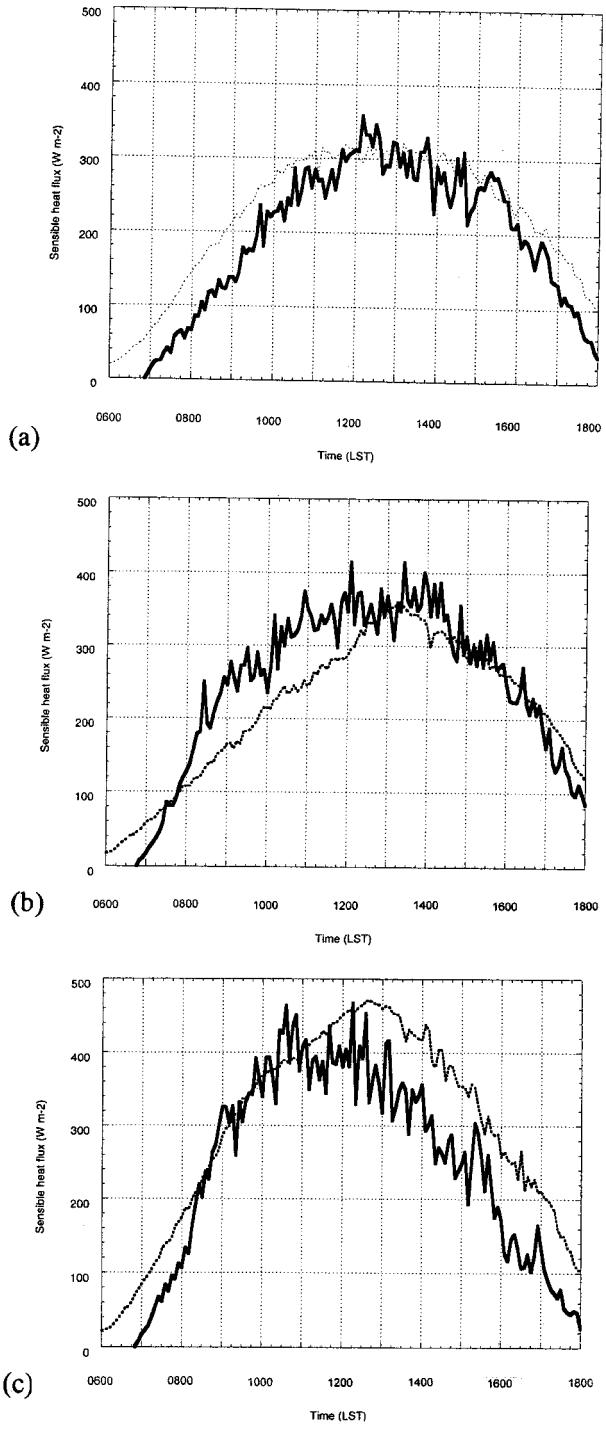

FIG. 17. Time series of modeled (dotted) and BC (solid) H at BEAV Mesonet site. Data are available at 5-min intervals: (a) 2 Jul, (b) 3 Jul, (c) 13 Jul.

but very well in the afternoon; the modeled values of H became positive earlier in the morning than did the BC values. There are two possible causes for this problem. First, as noted previously, the parameterization for R_n is valid only during the daytime; therefore presunrise values of R_n may be erroneous. Second, BC estimates of H are based on the air-temperature gradient between 1.5 and 9 m, and the model estimates are based on the gradient between z_{0h} and 1.5 m. In the early morning, the condition $T(z_{0h}) > T(1.5\text{ m})$ occurs before the condition $T(1.5\text{ m}) > T(9\text{ m})$. The latter problem probably is less significant than the former.

By 13 July (Fig. 17c), the modeled and BC time series were similar in the morning; on the other hand, during the afternoon, the modeled H was greater than BC's H by $\sim$100 W m^{-2}. The relatively dry conditions ended on 21 July; there was significant rain at BEAV (Fig. 18), which saturated the soil at 5-cm depth. There is therefore a significant reduction in BC's H between 13 and 25 July (Fig. 19a). The modeled H is also smaller, though, and follows the time series of BC's H very closely. The best comparison of the month occurs on 31 July (Fig. 19b).

During the 5 days when data were analyzed, the modeled values of H at BEAV during 0800–1400 LST (the early-morning data were not considered because of the positive bias noted earlier) have a negligible MBE and an rmse similar to that found for the R_n data verifications (Fig. 20). The model slightly underestimates (overestimates) H for small (large) magnitudes, because the slope of the regression line is less than unity.

At the NOWA site, there were only 2 days that qualified for analysis. On both days, the modeled H was very similar to BC's H during the morning hours (Fig. 21). In the afternoon, BC's H decreased rapidly, and the modeled H completed a nearly sinusoidal cycle. The reasons for this sharp drop-off in H in the afternoon are not known, because there were no frontal passages and no clouds during the day. Because R_n is parameterized accurately, however, LE and/or G must be underestimated during this time, because H is calculated as a residual in the energy-balance equation. Because R_n typically peaks near 1200 LST on a clear day, one would expect H to peak then as well. The peak in BC's H, however, occurs between 1000 and 1100 LST instead. Still, the maximum values of H are modeled well for these two days. Based on the limited verification data available, it is apparent that the model estimates of H are of reasonable quality.

The four surface energy fluxes were calculated at all 44 sites every 5 min throughout July 1997, and monthly average maps were analyzed at 1200 LST. A two-pass Barnes scheme with Gaussian weighting and a grid spacing of 25 km was used. The values from at least two Mesonet stations were used to calculate analyzed gridpoint values. The average values of R_n (Fig. 22a) range from 480 W m^{-2} in north central Oklahoma to 590 W m^{-2} in the eastern Oklahoma Panhandle, where there was less cloudiness. Here, G ranges from 40 W m^{-2} in the north-central part of the state to 120 W m^{-2} in the southwest (Fig. 22b), where there was plentiful soil moisture all month. The pattern of sensible heat flux exhibits three distinct regimes (Fig. 22c): H is low in

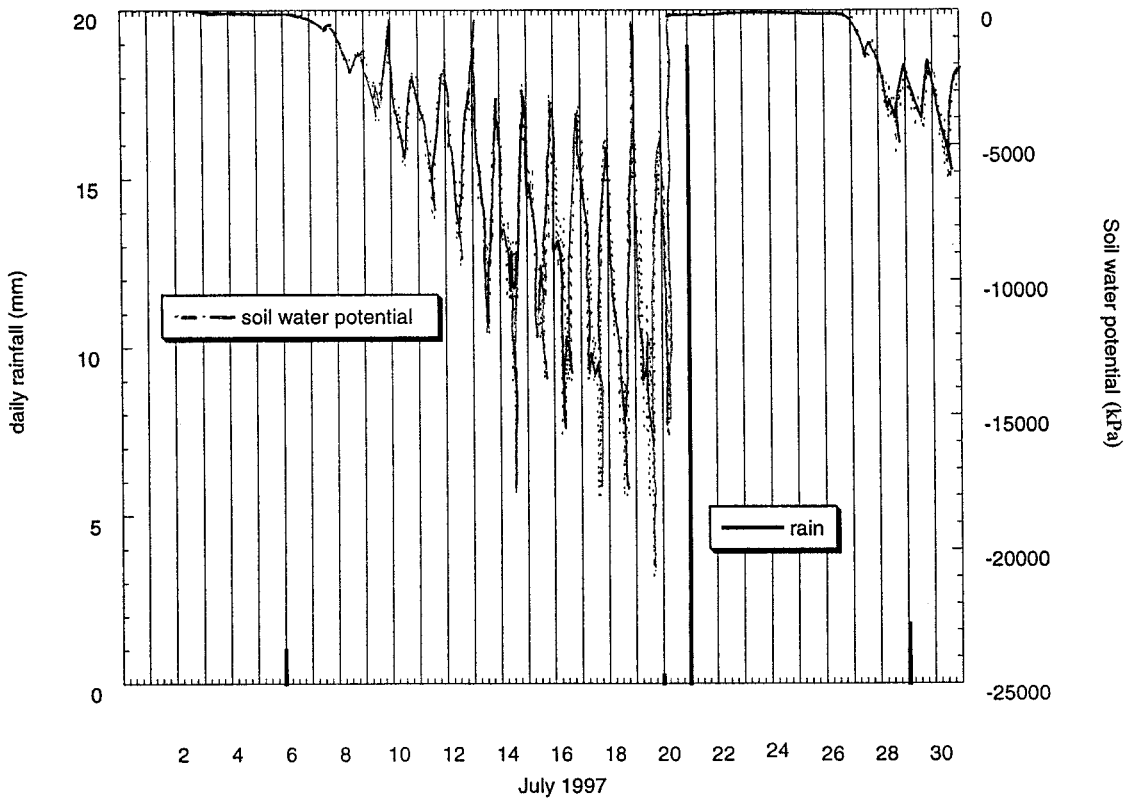

FIG. 18. Time series of soil-water potential and rainfall at the BEAV Mesonet site for Jul 1997.

the eastern half of the state where there is dense, green vegetation and large in northwest Oklahoma where the winter wheat has been harvested. Once this harvest has been completed in late May or early June, the heavily transpiring green wheat fields are transformed into piles of short, brown wheat stubble. The harvest has been shown to produce drastic changes in day-to-day weather, specifically, lower dewpoints and higher temperatures (Rabin et al. 1990). Then H is small in southwest Oklahoma where there was above-normal rainfall.

The patterns of LE are just the opposite of those of H (Fig. 22d). The largest values occur in the more-humid, eastern part of the state and in the southwest; the smallest values are found in the north-central part of the state near the harvested winter wheat fields. The overall patterns of the modeled energy fluxes are consistent with the land-use types and ambient atmospheric conditions during July 1997. It is important to note, however, that the model was tested only on clear days with wind speeds of at least 4 m s^{-1}. The model performance on days with clouds and/or light winds still is unclear, although Fig. 22 does suggest that the model is able to simulate at least the qualitative differences in surface fluxes across the state.

6. Summary and conclusions

A surface energy-budget model was developed to estimate surface fluxes in a dense network of surface instruments. A method was developed that requires only standard meteorological observations at one level. The inclusion of solar radiation and soil moisture observations (e.g., from the Oklahoma Mesonet) improves the ability to model surface fluxes. Of the four components of the surface energy balance, only R_n, G, and LE are calculated explicitly; H is computed as a residual.

To calculate R_n, four separate components are evaluated. The downwelling shortwave radiation is measured at the Mesonet sites, and the upwelling shortwave radiation is dependent upon a specification of albedo. The albedo parameterization was developed based on a climatological analysis of a typical annual albedo variation. This method provides for realistic spatial and temporal variations across Oklahoma.

Estimates of R_n were compared with direct measurements at the five enhanced Mesonet sites. The accuracy of the estimates was very good; mean bias errors were negligible and the rmses were only 18–26 W m^{-2}, which is about 5% of the total R_n. Accurate estimates of R_n are the most crucial part of the energy-budget model, because this quantity represents the total energy input to the surface.

Estimates of G were more difficult to verify, because the observations at the enhanced Mesonet sites did not include the storage term. The values of G measured at the ARM sites were significantly lower than the modeled values. The observations from the NORM site were of

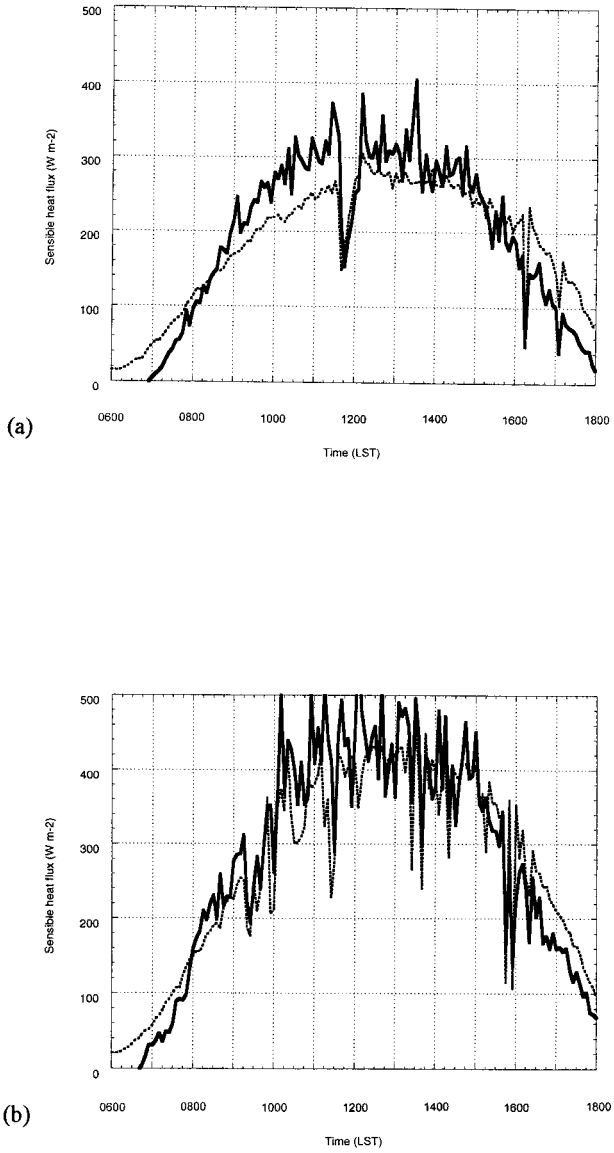

FIG. 19. Same as Fig. 17 except for (a) 25 Jul and (b) 31 Jul.

similar magnitude to the modeled values from the ARM sites, however. Evidence was found that the height of the vegetation significantly modulates the amount of net radiation that can reach the soil. To estimate G more accurately, instantaneous observations or estimates of vegetation height at the Mesonet sites are needed. Such observations currently are not available.

To get accurate estimates of H and LE with only one level of data, the Penman–Monteith (resistance) method must be used. An Ohm's-law analog is implemented to provide a conceptual model of the energy transfer near the surface. Formulations for aerodynamic and surface resistance also were developed. The aerodynamic resistance, which is a measure of the potential for turbulent vertical motion near the surface, is a function of the roughness length for momentum, the wind speed, and the stability. Monin–Obukhov similarity theory is used to develop this formulation.

The parameterization for surface resistance is crucial to the success of the model, because it determines how much of the available energy ($R_n - G$) is partitioned into LE and H. Previous studies have concluded that the surface resistance was related to many different atmospheric variables, including vapor-pressure deficit, air temperature, solar radiation, and soil moisture. These parameterizations also require estimates of variables that are not readily available, such as leaf area index and deep soil moisture, however. The simple parameterization developed here requires only those variables that are available in real time. Because direct observations of surface resistance are not readily available, it was retrieved by rearranging the Penman–Monteith equation and using ARM observations.

Data from the ARM sites in Lamont and Pawhuska were analyzed for one full growing season. It was found that r_s was linearly related to the vapor pressure deficit, because large values of r_s are associated with dry near-surface conditions and large values of vapor-pressure deficit. In addition to the vapor-pressure deficit dependence, r_s also was linearly related to the magnitude of solar radiation but only for dry near-surface conditions, because a plant typically will close its stomata in conditions of low light.

The surface resistance was found to be independent of air temperature except during very warm conditions ($T > 30$°C), when r_s decreases. The opening of the stomata on hot days may be a self-preservation mechanism similar to the sweating experienced by humans. Last, the relationship between r_s and soil moisture was examined. The amount of soil-water potential was shown to affect r_s only in very dry conditions (< -330 kPa). For dry soils, r_s increases significantly with the continued decrease in soil-water potential. In addition to the four aforementioned relationships, r_s varied sinusoidally at the Pawhuska site; minimum values were found in early July. Because this behavior was not found in the Lamont data, separate parameterizations of r_s were used for eastern and western Oklahoma. A simple linear combination of the four (five) relationships described above is used to parameterize r_s for western (eastern) Oklahoma. These parameterizations were unbiased and had rmses of 30 s m^{-1} and 45 s m^{-1} for western and eastern Oklahoma, representing approximately 30% and 45% errors, respectively. These values correspond to errors of $\sim$30 W m^{-2} (eastern) and $\sim$45 W m^{-2} (western) in the estimates of both LE and H, or a 10%–20% error. Future work will include comparison of this new r_s formulation with other commonly used formulation and a more-detailed investigation of the variation of r_s with vegetation type.

Observed values of H during July 1997 at two Mesonet sites (BEAV and NOWA) were used to verify our model. At BEAV, data collected during 5 clear, calm days were examined. The model values of H were un-

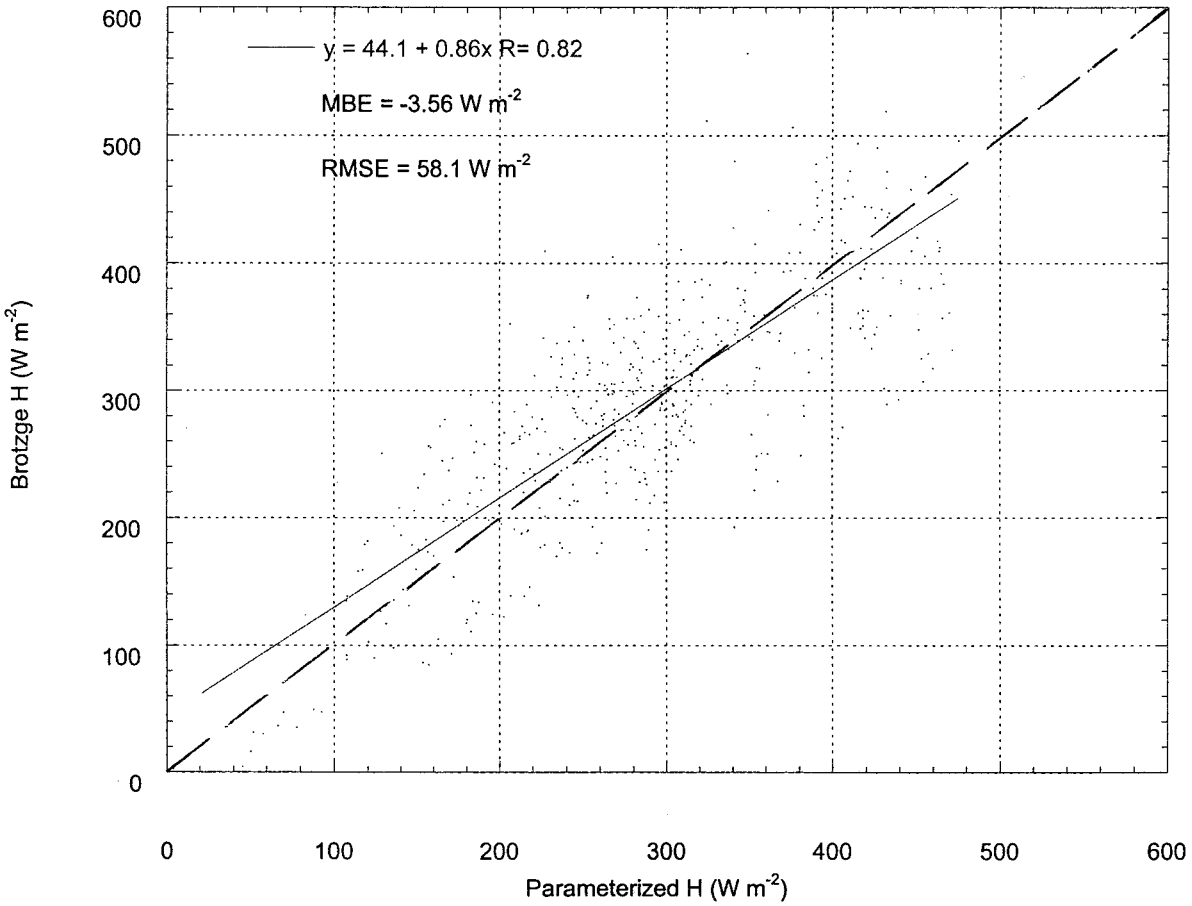

FIG. 20. Comparison of BC and calculated H at 5-min intervals from the daylight hours (0800–1600 LST) for 5 clear days with moderate wind in Jul 1997 at BEAV. The solid line represents the results of a linear regression, where R is the correlation coefficient. Mean bias errors and rmses are also given. The dashed line represents a perfect fit between the observed and calculated values.

biased, with rmses near 60 W m^{-2}. At the NOWA site, 2 days were examined. In both cases, the modeled H was similar to the observed H during the morning hours but was slightly larger in the afternoon. The limited amount of verification data currently available causes the model results to be preliminary. Within the next few years, instrumentation to measure surface energy fluxes directly will be installed at all of the Oklahoma Mesonet sites via the Oklahoma Atmospheric Surface-Layer Instrumentation System project (Brotzge et al. 1999). These data then will be used to test the model more rigorously.

Simple but important improvements in current operational and research models can be made using the tools developed here. For example, the Eta Model (Black et al. 1994) estimates of R_n exhibited a positive bias of ~100 W m^{-2} during May–July 1997 (C. Marshall 1998, personal communication), and the parameterized estimates are unbiased. This 100–W m^{-2} error in modeled R_n gets partitioned into the other three fluxes in the surface budget, eliminating any hope of accurately modeling sensible and latent heat fluxes. This excess energy, once it is distributed to the other fluxes, results in warmer and/or moister surface conditions in the model and therefore contributes to poor convection forecasts.

The Eta Model vegetation classification, used in determining the model-predicted surface resistance, considers most of the body of Oklahoma to have similar types of vegetation. Analysis of the observed behavior of surface resistance in this study contradicts this assumption, however; separate parameterizations for eastern and western Oklahoma are required. Last, Pan (1990) used a minimum value of r_s of 60 s m^{-1} for the scheme used in the National Centers for Environmental Prediction's (NCEP) medium-range forecast model. The results from this study suggest that this minimum value may vary considerably across a range of vegetation types.

Because the Mesonet measurements are made in open fields, there is some concern that they may not be representative of conditions in the surrounding area. In northwestern Oklahoma, for example, the early-spring land use pattern is dominated by green, heavily transpiring winter wheat surrounded by dormant, brown grasslands. Because Mesonet sites are not located in

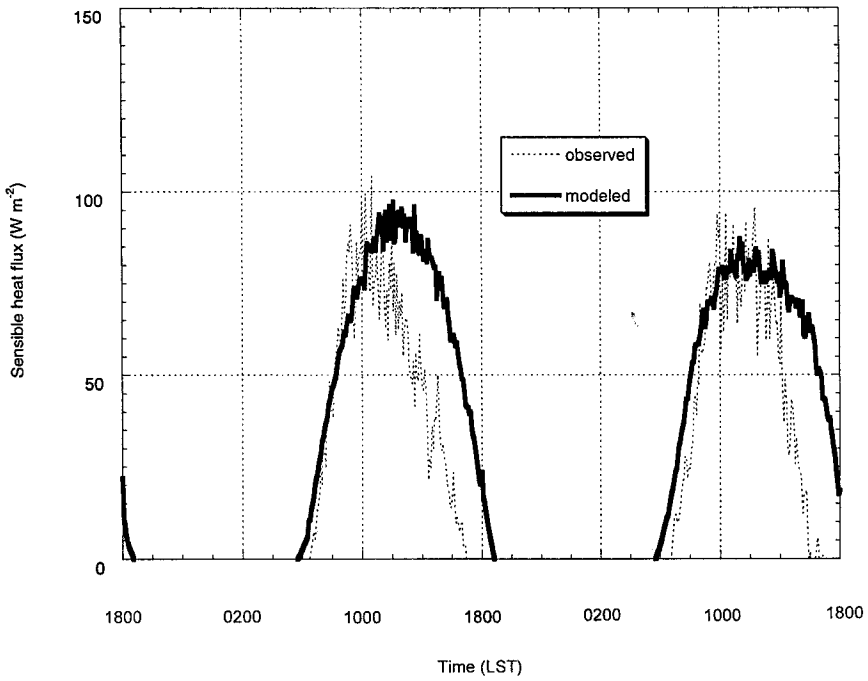

FIG. 21. Time series of observed (dashed) and calculated (solid) H at NOWA Mesonet site on 12–13 Jul 1997. Data are available at 5-min intervals.

these wheat fields, there is some trepidation that flux estimates made from these observations may not be representative of areal averages. Examination of temperatures and dewpoints does suggest that the effect of the wheat fields is detectable at nearby Mesonet sites, however. In this case, a broad swath of relatively lower temperatures and higher dewpoints is commonly observed on a clear, early-spring afternoon in the ''wheat belt.'' After the wheat is harvested in late spring, this signal is reversed, because the surrounding vegetation then is green. Higher temperatures and lower dewpoints then are noted in the same area. This result implies that the Mesonet data *are* representative, at least in this case, of the dominant land use pattern of the area.

There are several possible ways to improve model results. Real-time knowledge of vegetation height would allow for significant improvements in the estimation of G and, to a lesser extent, H and LE. Measurements of T_g, possibly with infrared thermometers, also would greatly improve estimates of G, H, and LE. Another way to improve the model would be to analyze a greater volume of ARM data so as to tune the r_s parameterization more finely.

Because existing land surface schemes are designed for modeling studies, the surface energy-budget model developed here is unique in its ability to predict fluxes in real time. Most of the parameterizations in the new model are simpler than those in existing schemes, but this simplicity allows for relatively easy application at any location with standard meteorological data. Based on the limited verification data used in this study, the new model shows promise in diagnosing real-time energy flux fields. The limitations of the model cannot be overlooked, however. The current version cannot diagnose the surface energy fluxes at night or when there is snow cover on the ground. Future upgrades to the model will address these issues.

The model can be used in a variety of ways. Correlations between the sensible heat flux gradients and local wind perturbations could be calculated to understand better the ''inland sea breeze'' (Sun and Ogura 1979). Calculated fluxes could be compared with those generated from numerical models. Variations in eastward dryline motion could be predicted based on the along-dryline variation of sensible heat flux. Predictions of evapotranspiration from hydrological models could be compared with the calculated latent heat flux. Last, the gradients in surface fluxes could be correlated to the locations of convection initiation. The surface energy budget model already is being used to calibrate remotely sensed data to understand better the first appearance of spring foliage, or the ''green wave'' (M. Schwartz 1999, personal communication).

Emanuel et al. (1995), in a report detailing ''intellectual challenges of the day that may lead to improvements in weather observations, forecasting, and warning,'' stressed the importance of gaining a better understanding of land–atmosphere interactions for applications in numerical modeling and weather forecasting. The results from this research will assist in achieving this rather lofty goal.

Acknowledgments. We thank the Oklahoma Climatological Survey (OCS) for providing the Mesonet data

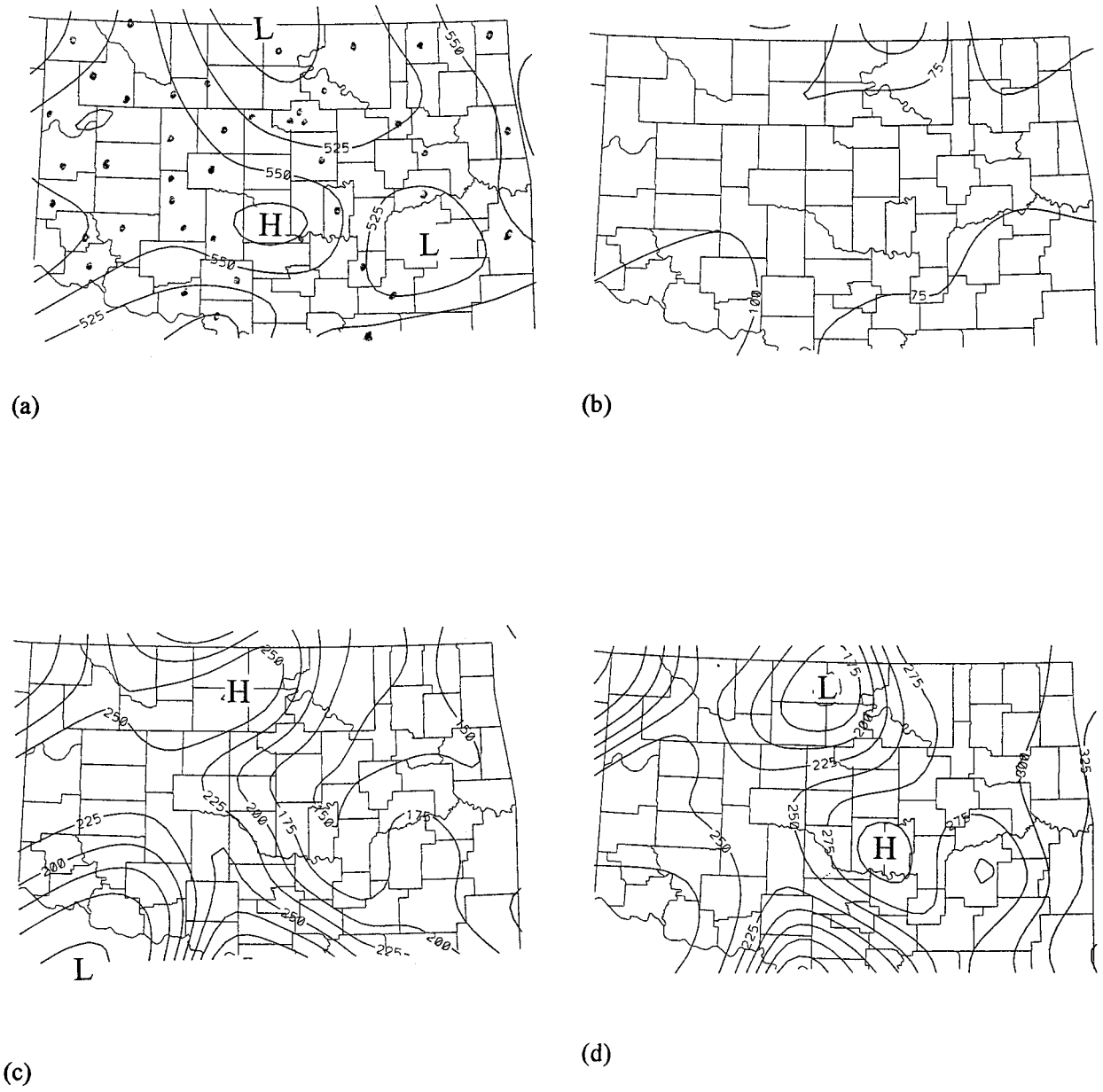

FIG. 22. Average calculated fluxes for Jul 1997 at 1200 LST. Contours are spaced at intervals of 25 W m^{-2}: (a) R_n, (b) G, (c) H, and (d) LE. Dots in (a) represent 44 stations that were used in the analysis.

and to Michael Splitt for ARM data and data support. The ARM program is sponsored by the U.S. Department of Energy, Office of Energy Research, Office of Health and Environmental Research, Environmental Sciences Division. Dale Morris of the School of Meteorology at the University of Oklahoma (OU) and Curtis Marshall (NCEP) provided much of the objective analysis and plotting software. Tim Hughes (OCS) provided the 229-L documentation and CSI calibration tests. Jeff Basara (OU) provided the 229-L ''raw'' data. Drs. David Stensrud, Ken Crawford, Claude Duchon, Karen Humes, and Conrad Ziegler also provided significant input into this research. This work was funded by NSF Grants ATM-9302379 and ATM-9612674.

REFERENCES

Al Nakshabandi, G. A., and H. Kohnke, 1965: Thermal conductivity and diffusivity of soils as related to moisture tension and other physical properties. *Agric. Meteor.*, **2,** 271–279.

Anthes, R. A., 1978: The height of the planetary boundary layer and the production of circulation in a sea breeze model. *J. Atmos. Sci.*, **35,** 1231–1239.

Arritt, R. W., 1989: Numerical modeling of the offshore extent of sea breezes. *Quart. J. Roy. Meteor. Soc.*, **115,** 547–570.

Basara, J. B., K. C. Crawford, and R. L. Elliott, 1998: In situ measurements of soil moisture from the Oklahoma Mesonet. Preprints, *10th Symp. on Meteorological Observations and Instrumentation*, Phoenix, AZ, Amer. Meteor. Soc., 301–306.

Berkowicz, R., and L. P. Prahm, 1982: Sensible heat flux estimated from routine meteorological data by the resistance method. *J. Appl. Meteor.*, **21,** 1845–1864.

Black, T., 1994: The new NMC mesoscale Eta Model: Description and forecast examples. *Wea. Forecasting*, **9,** 265–278.

Brock, F. V., K. C. Crawford, R. L. Elliott, G. W. Cuperus, S. J. Stadler, H. L. Johnson, and M. D. Eilts, 1995: The Oklahoma Mesonet: A technical overview. *J. Atmos. Oceanic Technol.*, **12,** 5–19.

Brotzge, J. A., and K. C. Crawford, 2000: Estimating sensible heat flux from the Oklahoma Mesonet. *J. Appl. Meteor.*, **39,** 102–116.

——, and Coauthors, 1999: The Oklahoma Atmospheric Surface-Layer Instrumentation System (OASIS) project. Preprints, *13th Symp. on Boundary Layers and Turbulence*, Dallas, TX, Amer. Meteor. Soc., 612–615.

Businger, J. A., W. F. Dabberdt, A. C. Delany, T. W. Horst, C. L. Martin, S. P. Oncley, and S. R. Semmer, 1990: The NCAR Atmosphere–Surface Turbulent Exchange Research (ASTER) Facility. *Bull. Amer. Meteor. Soc.*, **71,** 1006–1011.

Chen, T. H., and Coauthors, 1997: Cabauw experimental results from the Project for Intercomparison of Land-Surface Parameterization Schemes. *J. Climate*, **10,** 1194–1215.

Clapp, R. B., and G. M. Hornberger, 1978: Empirical equations for some soil hydraulic properties. *Water Resour. Res.*, **14,** 601–604.

Crawford, T. M., and H. B. Bluestein, 1997: Characteristics of dryline passage during COPS-91. *Mon. Wea. Rev.*, **125,** 463–477.

——, and C. E. Duchon, 1999: An improved parameterization for estimating downwelling longwave radiation at the earth's surface. *J. Appl. Meteor.*, **38,** 474–480.

de Vries, D. A., 1963: Thermal properties of soils. *Physics of Plant Environment*, W. R. Van Wijk, Ed., North-Holland, 337–347.

Dyer, A. J., 1974: A review of flux–profile relationships. *Bound.-Layer Meteor.*, **7,** 363–372.

Emanuel, K. A., and Coauthors, 1995: Report of the First Prospectus Development Team of the U.S. Weather Research Program to NOAA and the NSF. *Bull. Amer. Meteor. Soc.*, **76,** 1194–1208.

Gao, W., R. L. Coulter, B. M. Lesht, J. Qiu, and M. L. Wesely, 1998: Estimating clear-sky regional surface fluxes in the Southern Great Plains Atmospheric Radiation Measurement site with ground measurements and satellite observations. *J. Appl. Meteor.*, **37,** 5–22.

Garratt, J. R., 1992: *The Atmospheric Boundary Layer*. Cambridge University Press, 316 pp.

Halliwell, D. H., and W. R. Rouse, 1989: A comparison of sensible and latent heat flux calculations using Bowen ratio and aerodynamic methods. *J. Atmos. Oceanic Technol.*, **6,** 563–574.

Henderson-Sellers, A., A. J. Pitman, P. K. Love, P. Irannejad, and T. H. Chen, 1995: The Project for Intercomparison of Land Surface Parameterization Schemes (PILPS): Phases 2 and 3. *Bull. Amer. Meteor. Soc.*, **76,** 489–503.

Hjelmfelt, M., 1990: Numerical study of the influence of environmental conditions on lake-effect snowstorms on Lake Michigan. *Mon. Wea. Rev.*, **118,** 138–150.

Humes, K. S., W. P. Kustas, M. S. Moran, W. D. Nichols, and M. A. Weltz, 1994: Variability in emissivity and surface temperature over a sparsely vegetated surface. *Water Resour. Res.*, **30,** 1299–1310.

Lee, T. J., 1992: The impact of vegetation on the atmospheric boundary layer and convective storms. Paper 509, Department of Atmospheric Science, Colorado State University, 137 pp.

——, and R. A. Pielke, 1992: Estimating the soil surface specific humidity. *J. Appl. Meteor.*, **31,** 480–484.

Leese, J. A., 1993: Implementation plan for the GEWEX Continental-Scale International Project (GCIP). Int. GEWEX Project Office 6, 148 pp. [Available from International GEWEX Project Office, 1010 Wayne Ave., Suite 450, Silver Spring, MD 20910.]

Loveland, T. R., J. W. Merchant, D. O. Ohlen, and J. F. Brown, 1991: Development of a land-cover characteristics database for the conterminous U.S. *Photogr. Eng. Remote Sens.*, **57,** 1453–1463.

Marshall, T. J., J. W. Holmes, and C. W. Rose, 1996: *Soil Physics*. Cambridge University Press, 453 pp.

McGinley, J., 1986: Nowcasting mesoscale phenomena. *Mesoscale Meteorology and Forecasting*, P. S. Ray, Ed., Amer. Meteor. Soc., 657–688.

Monin, A. S., and A. M. Obukhov, 1954: Dimensionless characteristics of turbulence in the atmospheric surface layer (in Russian). *Dokl. Akad. Nauk. SSSR*, **93,** 223–226.

Monteith, J. L., 1965: Evaporation and environment. *Proceedings of the 19th Symposium of the Society for Experimental Biology*, Cambridge University Press, 205–235.

Niyogi, D. S., and S. Raman, 1997: Comparison of four different stomatal resistance schemes using FIFE observations. *J. Appl. Meteor.*, **36,** 903–917.

Oke, T. P., 1987: *Boundary Layer Climates.* 2d ed. Methuen, 435 pp.

Oklahoma Climatological Survey, 1994: A guide to interpreting Mesonet data. Oklahoma Climatological Survey, 20 pp. [Available from Oklahoma Climatological Survey, 100 E. Boyd St., Suite 1210, Norman, OK 73019.]

Pan, H.-L., 1990: A simple parameterization scheme of evapotranspiration over land for the NMC medium-range forecast model. *Mon. Wea. Rev.*, **118,** 2500–2512.

Paulson, C. A., 1970: The mathematical representation of wind and temperature profiles in the unstable atmospheric surface layer. *J. Appl. Meteor.*, **9,** 857–861.

Penman, H. L., 1948: Natural evaporation rates from open water, bare soil and grass. *Proc. Roy. Soc. London*, **194A,** 120–145.

Pielke, R. A., 1984: *Mesoscale Meteorological Modeling.* Academic Press, 612 pp.

Rabin, R. M., S. Stadler, P. J. Wetzel, D. J. Stensrud, and M. Gregory, 1990: Observed effects of landscape variability on convective clouds. *Bull. Amer. Meteor. Soc.*, **71,** 272–280.

Reece, C. F., 1996: Evaluation of a line heat dissipation sensor for measuring soil matric potential. *Soil Sci. Soc. Amer. J.*, **60,** 1022–1028.

Richman, M. B., and P. J. Lamb, 1985: Climatic pattern analysis of three- and seven-day summer rainfall in the central United States: Some methodological considerations and a regionalization. *J. Climate Appl. Meteor.*, **24,** 1325–1343.

Rutter, A. J., 1975: The hydrological cycle in vegetation. *Vegetation and the Atmosphere*, J. L. Monteith, Ed., Academic Press, 111–154.

Schmugge, T. J., and F. Becker, 1991: Remote sensing observations for the monitoring of land-surface fluxes and water budgets. *Land Surface Evaporation*, T. J. Schmugge and J. C. André, Eds., Springer-Verlag, 337–347.

Sousounis, P. J., and J. M. Fritsch, 1994: Lake-aggregate mesoscale disturbances. Part II: A case study of the effects on regional and synoptic-scale weather systems. *Bull. Amer. Meteor. Soc.*, **75,** 1793–1811.

Stokes, G. M., and S. E. Schwartz, 1994: The Atmospheric Radiation Measurement (ARM) Program: Programmatic background and design of the Cloud and Radiation Test Bed. *Bull. Amer. Meteor. Soc.*, **75,** 1201–1221.

Stull, R. B., 1986: *Boundary Layer Basics: A Survey of Boundary Layer Meteorology.* University of Wisconsin—Madison, 51 pp.

Sun, W.-Y., and Y. Ogura, 1979: Boundary-layer forcing as a possible trigger to a squall-line formation. *J. Atmos. Sci.*, **36,** 235–253.

Wieringa, J., 1993: Representative roughness parameters for homogeneous terrain. *Bound.-Layer Meteor.*, **63,** 323–363.

Xu, Q., B. Zhou, S. D. Burk, and E. H. Barker, 1999: An air–soil layer coupled scheme for computing surface heat fluxes. *J. Appl. Meteor.*, **38,** 211–223.

Zhou, B., and Q. Xu, 1999: Computing surface fluxes from Mesonet data. *J. Appl. Meteor.*, **38,** 1370–1383.

Ziegler, C. L., W. J. Martin, R. A. Pielke, and R. L. Walko, 1995: A modeling study of the dryline. *J. Atmos. Sci.*, **52,** 263–285.